NUMERICAL PREDICTION OF TURBULENT BOUNDARY LAYER IN TRANSITION FROM SMOOTH TO ROUGH SURFACE

BY

MD. MAHMUD HOSSAIN BISWAS

A Thesis Submitted to the Department of Mechanical Engineering in Partial Fulfilment of the Requirements for the Degree of

Master of Science
in
Mechanical Engineering

JULY 1992

BANGLADESH UNIVERSITY OF ENGINEERING AND TECHNOLOGY
DHAKA-1000, BANGLADESH

NUMERICAL PREDICTION OF TURBULENT BOUNDARY LAYER IN TRANSITION FROM SMOOTH TO ROUGH SURFACE

A THESIS

BY

MD. MAHMUD HOSSAIN BISWAS

Approved as to style and content by:

(Dr J.A. Naser)
Assistant Professor
Department of Mechanical Engineering
BUET, Dhaka-1000 : Chairman

(Dr Wahhaj Uddin)
Professor & Head
Department of Mechanical Engineering
BUET, Dhaka-1000 : Member (Ex-officio)

(Dr M.A. Taher Ali)
Professor
Department of Mechanical Engineering
BUET, Dhaka-1000 : Member

(Dr A.K.M.Sadrul Islam)
Associate Professor
Department of Mechanical Engineering
BUET, Dhaka-1000 : Member

(Dr Muhammed Ali Bhuiyan)
Assistant Professor
Department of Water Resources Engineering
BUET, Dhaka-1000 : Member (External)

CERTIFICATE OF RESEARCH

This is to certify that the work presented in this thesis is the outcome of the investigations carried out by the candidate under the supervision of Dr. J. A. Naser in the Department of Mechanical Engineering of Bangladesh Universtity of Engineering and Technology, Dhaka1000, Bangladesh

Superviser

Candidate

ABSTRACT

The thesis describes a computational investigation of turbulent boundary layer in transition from smooth to rough surface. The scope of the present computational study is limited to numerical prediction of the flow parameters of steady two dimensional turbulent flow over smooth to rough surface at different Reynolds numbers. "TEACH-T", a general computer programme has been used for this purpose.

The governing partial differential equations expressed in cartesian co-ordinate system are discretised in a finite difference technique. A staggered arrangement of variables has been used in conjunction with the SIMPLE algorithm. The upwind differencing scheme is employed to evaluate the convective terms.

The time averaged governing equations of mean flow is closed using the standard k-ε turbulence model.

The surface texture of the rough portion used in experiment is simulated in the present computation in two different ways (i) Mean height type: computational cells of total height equal to the height of the average stone chips used in the experiment are continuously blocked off to incorporate the rough surface into the flow domain. (ii) Saw tooth type: computational cells are blocked off in such a way that the blocked cells give the bottom surface a saw tooth type configuration with the saw tooth height equal to the average stone chips height.

The prediction is in good agreement with the experimental data in the smooth surface. Whereas, in the rough surface: for mean height type; the velocity profiles conform with the experimental data but pressure gradient is under predicted, for saw tooth type; pressure gradient conform with the experimental data but velocity profile is under predicted .

ACKNOWLEDGEMENTS

The author is highly grateful and indebted to his Superviser, Dr. J.A. Naser, Assistant Professor, Department of Mechanical Engineering, BUET, Dhaka for his careful supervision, constant inspiration, unceasing encouragement, invaluable suggestions and untiring support throughout the research work.

The author pays his sincere gratitude to Dr. S.M.Nazrul Islam, Professor, Department of Mechanical Engineering, BUET and Dr. Wahhaj Uddin, Professor, and Head of the same department for their co-operation.

The author is especially indebted to Prof. Dr. M. Nurul Islam, Director, IAT, BUET, for allowing him to continue his work and providing him continuous encouragement and invaluable suggestions at different phases of the work.

The author gratefully acknowledges the assistance received from Mr. Mrinal Kanti Shaha, Lecturer, Department of Mechanical Engineering, BUET and Mr. Md. Maniruzzaman, Assistant Professor of the same department during running his computer programme.

Thanks are due to Md. Abdul Wohab Laskar and Md. Ilias Zabed for typing this thesis.

Lastly, the author would like to express his sincere thanks to all others, who directly or indirectly have helped him in completing the work properly.

To my Parents

TABLE OF CONTENTS

Title		Page
Certificate of Approval		
Certificate of Research		
Abstract		i
Acknowledgements		ii
Dedication		iii
Table of Contents		iv
List of Symbols		vii
List of Figures		x
CHAPTER-I	INTRODUCTION	1
1.1	Backgroun	1
1.2	Motivation Behind the Selection of the Study	3
1.3	Importance of Numerical Investigation	5
1.4	The Problems and Objectives	6
15	The Present Contribution	7
1.6	Thesis Outline	7
CHAPTER-II	LITERATURE REVIEW	9
2.1	General	9
2.2	Literature On Turbulent Flow Over Smooth Surface	9
2.3	Literature On Turbulent Flows Over Rough Surfaces	12
	2.3.1 Turbulent Flow Through Rough Pipes	12
	2.3.2 Turbulent Flow Through Rough Ducts and Channels	14
2.4	Literature On Turbulent Flows Through Pipes, Ducts and Channels with Change in Surface Roughness	16
CHAPTER-III	GOVERNING DIFFERENTIAL EQUATIONS	20
3.1	Introduction	20
3.2	Transport Equations	21
	3.2.1 Governing Differential Equations in General Co-ordinate	21

3.2.2 The Form of Governing Differential Equations Adopted for Use in This Study 22

3.3 Turbulence Modelling 23

3.3.1 Introduction 23
3.3.2 Turbulence Model for the Present Study 29

CHAPTER-IV NUMERICAL SOLUTION 33

4.1 Introduction 33
4.2 Expanded Form of Governing Differential Equations 34
4.3 The Method of Discretization 34
4.4 Differencing Scheme 36

4.4.1 Choice of Differencing Schemes 36
4.4.2 Brief Review of Some Differencing Schemes 38

4.5 Solution Procedure 42

4.5.1 Grid & Variable Arrangement 42
4.5.2 Calculation of Pressure 42

4.6 Boundary Conditions 45

4.6.1 On the Basis of Wall Boundary Conditions 46
4.6.2 Incorporation of Wall Boundary Condition 50

4.7 Solution Algorithm 53

CHAPTER-V RESULTS AND DISCUSSIONS 55

5.1 Introduction 55

5.2 Flow Configuration 56
5.3 Domain of Solution and Computational Grid 56
5.4 Boundary Conditions 57

5.4.1 Inlet Conditions 57
5.4.2 Outlet Condition 58

5.5 Grid Dependence Test 58
5.6 Presentation of Results and Comparison with Experiment 58
5.7 Discussions 63

CHAPTER-VI SUMMARY AND CONCLUSIONS 67

6.1 General 67
6.2 Summary of Main Findings and Achievements 67
6.3 Suggestions for Future Work 68

REFERENCES 70

FIGURES 75

APPENDIX-A 93

APPENDIX-B 94

LIST OF SYMBOLS

Symbol	Meaning
Latin Letters:	
A	Constant in log-law of the wall
b	Constant
c	Constant
C_f	Co-efficient of friction $\tau/.5\rho u^2$
C_μ	Eddy viscosity factor
Cε1	Dimensionless constant
$C_{\varepsilon 1}$	Dimensionless constant
D	Deformation or rate of strain tensor
D_t	Width of the test section
D/Dt	Total derivative
E	Intregration constant
G	Turbulent energy production rate
I	Turbulent intensity
K	Absolute height of roughness
k	Turbulent kinetic-energy
l	Length scale represents the size of the turbulent eddies
M_p	Mass source
p	Pressure
q	Scaler flux
Re	Reynolds number, $\rho u D_t/\mu$

r	Radius of a pipe
S	Source term in conservation equation
T	Stress tensor
U	Axial free-stream velocity
u	Mean axial velocity
u_l	Longitudinal component of rms of fluctuation of velocity
u^*	Friction velocity
u^+	Non-dimensional velocity, u/u^*
u_τ	Shear velocity
v'	Transuverse component of rms of fluctuation of velocity
x	Axial distance measured from smooth rough junction
y	Vertical distance from the bottom surface of the wall
y^+	Non-dimensional distance, yu^*/ν

Greek Letters:

Γ	Circulation, molecular or turbulent diffusivity of scalar Quantaties
Δ	Difference of argument
$\delta/\delta t$	Partial derivative with respect time
$\delta/\delta x$	Partial derivative with respect to space
μ	Molecular viscosity of air
μ_t	Turbulent viscosity
μ_{eff}	Effective viscosity

ν	Kinematic viscosity of air
ρ	Density of air
τ	Shear stress
τ_o	Shear stress at surface
τ_w	Local wall shear stress
τI	Shear stress in inertial sublayer
λ	Length scale factor (= 0.005)
ε	Turbulent kinetic-energy dissipation rate
ν_t	Eddy (turbulent) kinmatic viscosity
K	Vonkarman constant (= 0.4187)
σk	Dimensionaless constant
σ_ε	Dimensionaless constant
ϕ	Basic dependent variable

SUBSCRIPT

i,j	Tensor subscript: terms in which a subscript appears twice are summed over all value (1,2,3) of that subscript.

SUPERSCRIPT

'	Instantaneous value

LIST OF FIGURES

Figure No.	Name	Page No.
Fig. 1	Experimental test section of Naser (1985)	75
Fig. 2(a)	Computational Grid (Saw Tooth Type)	76
Fig. 2.(b)	Computational Grid (Mean Height Type)	77
Fig. 3.1	Two dimensional computational cell	78
Fig. 3.2	Control Volume for Continuity Equation	78
Fig. 3.3	Control Volume for U	79
Fig. 3.4	Control Volume for V	79
Fig. 3.5	Computational grid, location and control volumes (cells) of scalar variables and axial and radial velocities	80
Fig. 3.6	Schemiatic presentation of CDS	81
Fig. 3.7	Schemiatic presentation of UDS	81
Fig. 3.8	Schemiatic presentation of LUDS	81
Fig. 3.9	Incorporation of wall boundary condition for Momentum equation	82
Fig. 3.10	Incorporation of wall boundary condition for turbulence energy	82
Fig. 4.1(a)	Mean velocity profile over smooth surface at $x/D_t = -0.25$	83
Fig. 4.1(b)	Mean velocity profile over smooth surface at $x/D_t = -1.167$	84
Fig. 4.2	Mean velocity profile (over the entire-diameter) over smooth surface at $x/D_t = -0.83$	85
Fig. 4.3	Mean velocity profile over rough surface	86
Fig. 4.4(a)	Pressure Gradient along the direction of flow (Saw tooth)	94

Fig. 4.4(b)	Pressure Gradient along the direction of flow (Mean height)	95
Fig. 4.5	Friction factor Vs Reynolds number for smooth surface	96
Fig. 4.6	Friction factor Vs Reynolds number for Rough surface	97
Fig. 4.7	Logarithmic velocity Profile near the smooth surface	98
Fig. 4.8(a)	Logarithmic velocity Profile over the rough surface (Saw-tooth)	100
Fig. 4.8(b)	Logarithmic velocity Profile over the rough surface (Mean-height)	101
Appendix A:	Overall Structure of the Mathematical Foundation	102
Appendix B:	Overall Structure of Teach-T	103

CHAPTER-I

INTRODUCTION

1.1 Background

When a flow comes in contact with a surface, it forms a so called boundary layer in the most immediate vicinity of the contact zone. For turbulent flows, a turbulent boundary layer forms whenever the flow encounters a surface. The knowledge about the boundary layer is of prime importance for the study of a transport phenomenon, because transactions of shear, heat, momentum, kinetic energy, etc., mainly take place within this zone.

The term "turbulent flows" are characterised by random, irregular, fluctuating flows superimposed upon the main stream . According to Hinze [1975] "Turbulent fluid motion is an irregular condition of flow in which the various quantities show a random variation with time and space coordinates, so that statistically distinct average values can be discerned". The fluctuation which is superimposed on the principal motion is so complex in its details that it seems to be inaccessible to mathematical treatment, but it must be realized that, the resulting mixing motion is very important for the course of flow and for equilibrium of forces. These fluctuations are mainly responsible for the large resistance experienced by turbulent flows in pipes or other closed conduits, for drag encountered by the ships, and airplanes, and contribute chiefly to the losses in turbomachines. On the

other hand, it enables us to achieve greater pressure increase in diffusers or along aeroplane wings and compressor blades.

Inspite of its variety of occurrence and applications, many aspects are not yet known about turbulent flow structure because of its almost inaccessibility of mathematical treatment, on the contrary, laminar flow is strictly mathematical and its governing differential equation can be written exactly and can be solved easily by high speed and super computers.

But turbulent flow poises a different problem with the impossibility of formulating exact boundary layer equations because of the presence of additional terms involving the time mean of the product of fluctuating velocities known as the Reynolds stress in the stress tensor.

However, attempts have been made to create a mathematical basis for the investigation of turbulent motion coupled with semi-empirical formulations. These endeavour ranges from simple mixing length hypothesis of prandtl to the solution of conservation equations for third order correlation by Launder and Spalding [1972] which envisaged properly dealing with the extra term mentioned above. The success in obtaining accurate turbulent flow predictions depends on prescribing a closed set of equations adequately accounting for the flow process.

For devising a suitable turbulence model for the complex correlations in the governing conservation equations, certain assumptions are made which need to be

supplemented by theoretical reasoning and empirical facts which, if accurate enough within the range of interest, will lead to correct prediction of turbulent flows.

Though experimental study of turbulent flow is a must for its correct prediction a full fledged experiment on turbulence is generally laborious, expensive, and very much time consuming. So other methods of investigations are often looked for. After the inception of high speed digital computers, numerical solution coupled with semi-empirical result has become a useful way of dealing with turbulence. To acquire an insight of turbulence process, computational method has gained much importance recently.

1.2 Motivation Behind the Selection of the Study

Turbulent fluid flows are most common in engineering arena and also in nature. Flows in water lines, oil pipelines, heat exchanger, nuclear reactors, air conditioning system, chemical processing plants, rotating machinery, etc., are the common example of turbulent flow over rough surface at least at higher Reynolds numbers. The system of some of the above installations are deliberately made rough to drive maximum economic benefits and to ensure better performance.

The change of surface roughness occurs both in engineering application and in nature. In the day to day application, flow encounters surface roughness change mainly due to change of new pipes for old one of different specifications. In this

cases, differential surface roughness causes development of different types of boundary layer which causes different rate of friction loss and heat transfer co-efficient.

Flows with dissimilar surface conditions, appear in many practical situation. Where technological requirements impose dissimilar boundary condition, such as in nuclear reactors, by making the surface of rod bundles rough, heat transfer rate between the coolant and the fuel can sufficiently be increased with relatively less increase of overall flow resistance.

In nature the change of surface roughness is frequently observed in flow through rivers and canals while they pass through different geological structures. Since flood alleviation schemes are the focus of much engineering works, the prediction of the conveyance capacity, velocity distribution and boundary shear stress in such channels is clearly important. The boundary shear stress distribution is a prerequisite for studies on bank protection and sediment transport.

Also sudden and frequent change in roughness is found in natural terrain where flowing wind encounters, hills, ditches, meadows, forests, villages, etc. All these surface configurations lie within the atmospheric boundary layer of the earth's surface. The influence of strong wind or storm on the earth surface is more severely felt in the boundary layer and the effect depends on the nature of the boundary layer growth rather than the free stream atmospheric air, which occurs high above the human habitation zone.

The coastal areas of Bangladesh is hit by cyclone almost every year causing loss of valuable lives and properties. The extent of damage can be reduced by understanding the behaviour of boundary layer and thereby prescribing methods of reducing the flow velocity within the atmospheric boundary layer.

It is against this background the present research work has been embarked upon. It is aimed at studying the changes happening in the boundary layer undergoing a sudden transition over a flat surface due to an upstanding intervention of roughness with comparatively high roughness ratio. This is expected to be a new type of flow situation with strong relevance to the cases of natural flows and flows of engineering interests. The present research is expected to reveal some important flow characteristics valuable for greater understanding of turbulent boundary layer and turbulence structure for the flow over varying surface roughness.

1.3 Importance of Numerical Investigation

In the recent past, the emergence of faster digital computers together with the development of more versatile and efficient numerical solution method has led to a substantial increase in the assembly of mathematical modelling of turbulent flow process. Now a days, in the field of engineering design of flow related technology, designers are looking for computational investigations to seek the optimum design,as experiments with either model or full scale prototype are generally laborious, expensive, and time dependent.

In the field of aerodynamics, the role of computational prediction method is worth mentioning. In the calculation of aerodynamic forces, experienced by space vehicle, the full scale model can be brought under practical situation only by the means of computational simulation.

The power of prediction enables us to operate existing equipment more safely and efficiently. Prediction of the relevant process help us in forecasting and even controlling potential dangers such as floods, cyclones, tides etc. These predictions offer economic benefits and contribute to human well being.

1.4 The Problems and Objectives

It is evident from the above discussion that dissimilar surface condition is of ever growing practical importance in the modern flow related technology. Considerable works have been done on flow over smooth to rough surface experimentally but comparatively a little attention has so far been focused on to predict turbulent flow over this type of surface condition computationally.

The objective of the present research work is therefore to extend a numerical procedure with view to developing a tool for investigating turbulent flows in the transition zone of smooth to rough surface.

The accuracy of prediction is assessed through comparison with experimental work of Naser [1985].

1.5 The Present Contribution

The present research study only covers the numerical investigation of the flow parameters of steady two dimensional turbulent flow over smooth to rough surface at different Reynolds numbers.

The specific contribution of this study are the following: Numerical Prediction of

a. velocity components
b. pressure gradient and its distribution
c. turbulence parameters
d. shear stress
e. boundary layer parameter
f. log-law parameters
g. assessment of the quality of numerical prediction through comparison with the experimental data.

1.6 Thesis Outline

In Chapter 2, a brief review of the investigations carried out by different researchers in the field of turbulent flow over dissimilar surface condition is presented.

In Chapter 3, the governing transport equations are presented. A brief review of the different approaches to the turbulence "closure problem" is given next. Then the chosen closure model for the present study is presented.

Chapter 4, presents the numerical solution method embodied in the present study. After presenting the expanded form of the governing differential equations, the discretization procedure is given. Then the differencing schemes used to evaluate various terms in the discretized equations are discussed from the point of view of numerical stability, accuracy and economy and accordingly choice is made. The grid and variable arrangement and the pressure correction equation that links the momentum and continuity equation are described next. Then, after presenting the treatment of boundary conditions, the solution algorithm is outlined.

In chapter 5, the computational results are presented and compared with the experimental results obtained by Naser [1985].

Finally, in Chapter 6, the main achievements of the thesis are summarized and recommendations are made for future work.

CHAPTER-II

LITERATURE REVIEW

2.1 General

Since the identification of turbulent flow by Osborne Reynolds, the researchers have devoted themselves to developing hypothesis, analytical methods and experimental investigations technique for the advancement of knowledge about turbulent flow. Recently, with the introduction of high speed digital computer, computational investigation of turbulent flow has opened up a new dimension to this field. A brief review of the contributions made by the worldwide researchers on turbulent flow, which are related to the present study and play a vital role in the development of this branch of physical science, is given below.

2.2 Literature on Turbulent Flow Over Smooth Surface

In the initial stage of research on turbulent flows, the researchers devoted themselves mainly to the study of flow over smooth surfaces. Blasius (1913), Stanton and Panel (1915), Schiller (1923), Hermann (1930), Nikuradse (1932), are some of the earliest investigators who worked on turbulent flow through smooth pipes.

Richard (1938) made some of the earliest measurements of turbulence parameters. He measured the longitudinal and transverse components of fluctuating velocity u' and v' and found that rise of u' was steep near the wall and was four times v'.

Laufer (1951) presented a detail exploration of the flow field of mean and fluctuating quantities in a two-dimensional channel flow. He confirmed the findings of Reichard except that rise of u' was less near the wall.

Klebanoff (1954) measured the three fluctuating components of velocity in a boundary layer along a smooth wall with zero pressure gradient. He noticed isotropic behaviour of turbulence intensities near the free stream but degree of anisotropy increased towards the wall.

Clark (1968) made an elaborate study of turbulent boundary layer in a 25.0 ft. long, 5.0 inch. wide channel section with aspect ration 12:1. Measurements were done at Reynolds number ranging from 10,000 to 1,30,000 based on channel half width and the centre line velocity. Mean velocity profiles were studied in every details and all the three fluctuating components of velocity along with frequency spectral analysis were investigated.

Thomas and Easter (1972) measured axial velocity, friction factor and wall shear stress in an 8.1 m. long square section duct of size 101.6 mm with the help of a DISA hot film pressure transducer. He correlated the friction factor with Reynolds number as:

$$C_f = 0.079 \times Re^{-0.25} \quad \ldots\ldots\ldots\ldots\ldots\ldots (2.2.1)$$

The Reynolds number in the experiment varied from 0.43 X 10^5 to 1.90 X 10^5 based on the hydraulic diameter of the duct and centre line velocity.

Patankar (1972) introduced a new dimension in the field of computational investigation of fluid flow problem. He succeeded in the prediction of laminar and turbulent flow through rectangular and triangular ducts using computational investigation technique.

The first successful attempt to predict the fully developed flow in a square duct was made by Launder and Ying (1973) with a single equation model coupled with "algebraic stress model". They demonstrated that the mean velocity field can be predicted fairly well by their algebraic stress model. However, no comparison of the computation and the experiment was made on the individual Reynolds stress component. Their innovative numerical work on the secondary flow prediction was followed by several other studies to calculate fully developed flow in some other non circular geometries. For example those of Aly, Trupp and Gerrard (1978) and Gosman and Raplay (1978) for an equilateral triangular duct and Caragilescov and Todress (1975) for triangular rod bundle. This algebraic stress model was effective for prediction of mean flow quantities. None of this studies revealed the details of the model performance on the local structure of turbulence.

Gosman and Ideriah (1976) computed turbulent flow through duct with sudden change in diameter and compared the result with experimental data.The comparison showed a good agreement.

Anderson, Tannehill and Pletcher (1984) carried out investigation in the prediction of turbulent flows and attained a great success.

Nakayama (1986) made a computational studies on turbulent flow through duct for his doctoral thesis and presented a series of comparison between experiment and prediction in three dimensional co-ordinate system showing good agreement between the compared values.

2.3 Literature on Turbulent Flows Over Rough Surfaces.

The earliest researchers who paid their attention to the effects of surface roughness on turbulent flow are Schiller (1923), Nikuradse (1930) and Streeter (1935). Moody's (1944) works formed the basis of studying turbulent fluid motion in relation to the surface condition. Some of the related important research works are presented below on the flows through pipes, rectangular ducts or channels.

2.3.1 Turbulent Flow Through Rough Pipes

Nikuradse (1950) was one of the pioneer workers in the field of turbulent flow through rough pipes. He pointed out that velocity distribution in a rough pipe

were progressively lowered from the smooth pipe relation as the Reynolds number increased. He performed extensive work on sand roughened pipe flow and formulated a volume of empirical relations between surface roughness and friction velocity.

Clauser (1956) studied the influence of roughness on the velocity distribution for flow through pipes. He observed a vertical shift of rough wall log-law profile from that of smooth wall and postulated a velocity distribution near the rough wall as,

$$\frac{u}{u^*} = 5.6 \log \frac{yu^*}{\nu} + 5.6 - \frac{\Delta u}{u^*} \quad \ldots\ldots\ldots (2.3.1)$$

The last term on the right hand side of the equation (2.3.1) is known as the wall function which takes into account the shift of the velocity profile from that of the smooth wall.

Robestson (1957) utilized Nikuradese's data and put forward a relation for the wall function as,

$$\frac{\Delta u}{u^*} = 5.6 \log \frac{ku^*}{\nu} - 2.7 \quad \ldots\ldots\ldots (2.3.2)$$

Equations (2.3.1) and (2.3.2) give,

$$\frac{u}{u^*} = 5.6 \log \frac{y}{k} + 8.3 \ldots\ldots\ldots\ldots (2.3.3)$$

Lawn and Hamlin (1968) made detail measurements of velocity in an internally roughened pipe. They found that flow over a fully rough surface was very much influenced by viscosity.

Towns et al (1972) performed a comprehensive experiment on turbulent flows through sand roughened pipes and proposed a velocity distribution of the form

$$\frac{u}{u^*} = 2.75 \ln \frac{yu^*}{\nu} + 4.55 \ldots\ldots (2.3.4)$$

which agrees very well with the experimental data for $yu^*/\upsilon > 70$.

2.3.2 Turbulent Flow Through Rough Ducts and Channels

Perry and Joubert (1963) performed experiments on rough surfaces with adverse pressure gradients to compare the results of the boundary layers with theory and with results of zero pressure gradient flow. They used wind tunnel test section measuring 5.5 ft.x4.25 ft.at the down stream end. Discrete rib roughness of height 0.125 inch and pitch 0.50 inch were used. They proposed a method of finding out the position of origin of vertical distance for rough wall flow. They found that the roughness function was independent of imposed pressure gradient.

Perry et al (1969) presented a detailed experimental study of turbulent boundary layer development over rough wall in both zero and adverse pressure gradients. The experiments were done in a wind tunnel test section of Perry and Joubert (1963). Roughness elements were of 1/8 inch, 1/2 inch and 1 inch height and of k-type and d-type (origin of the rough surface is located nither at the crest nor at the roots of the roughness elements but somewhere in the middle. Different researchers used different methods to find the origin of the rough surface. As a result, error always existed. When the error in the origin is proportional to the height of the roughness elements, the roughness is called k-type or sand roughness and when the error in origin is a linear function of the distance in the downstream direction, the roughness is called d-type roughness). Velocity profiles were measured and wall function was determined. The skin friction was calculated from pressure gradient measured by tapping the roughness elements and considering their form drag. Roughness function was found to be a function of length scale w. For k-type rough wall, w was proportional to roughness scale k and for d-type roughness it was postulated to be proportional to boundary layer thickness.

Wood and Antonia (1975) conducted elaborate experiments on the turbulent boundary layer over a d-type surface roughness similar to those used by Perry et al (1969) with $\lambda/k=2$. The boundary layer was found to satisfy self-preservation characteristics after $x/D_h=1.5$. The measurements included shear stress, turbulence intensities, turbulence frequency spectra and the analysis also included roughness function, dissipation of energy and flow visualization. Distribution of Reynolds normal and shear stresses across the boundary layer were found closely similar

to those found over a smooth surface (excepting the region immediately above the grooves).

2.4 Literature on Turbulent Flows Through Pipes, Ducts and Channels with Change in Surface Roughness

Jacobs (1939) was the pioneer in the investigation of turbulent flow through a duct with step change in surface roughness. He performed the study in a 60 cm X 20 cm channel with its floor fitted with discrete rib type roughness of height 1 mm and 8 mm pitch. He calculated the shear stress in the transition zone using the velocity distribution obtained from Prandtl's mixing length equation.

Clauser (1956) made a similar investigation like Jacobs on a flat plate in a constant pressure boundary layer and obtained a similar result.

Logans and Jones (1963) were the pioneer in the investigation of turbulent flow through pipe across a transition zone of surface roughness. They used a 8.0 inch diameter pipe, internally roughened by sand grains with r/k = 55. They reported that the shear stress suddenly increased at the rough smooth junction and remained constant throughout the transition zone.

Antonia and Luxton (1971) investigated the turbulent boundary layer in a depressed change of surface roughness in a zero pressure gradient flow. The velocity profile, shear stress and turbulence intensities were measured. They found the growth rate of internal boundary layer similar to that of zero pressure

gradient boundary layer. The turbulence level was found to be high inside the internal layer because of the large energy production near the rough wall. Antonia and Luxton performed another experiment in the same experimental set up but the direction of flow was reversed from rough to smooth.They measured all the mean values of turbulence parameters. The growth rate of internal boundary layer was found to be less than that for the smooth to rough change of surface roughness.

Antonia and Luxton (1971) measured the flow field down stream of an upstanding k-type roughness. The growth of the internal boundary layer was measured from u versus $y^{1/2}$ plot. They also measured longitudinal and transverse components of turbulence intensities, Reynolds shear stress, frequency spectra analysis of turbulence and auto and cross coefficients of turbulence intensities.

Carper (1972) measured turbulence intensities and co-relation co-efficient in turbulent flow of air in transition from smooth to a rough wall in a two dimensional channel of size 4.0 in.x46.5 in. Discrete rectangular ribs of height 0.281 in. and width 0.437 in. were placed at an interval of 8 inches on both the walls of the rough section. He observed that the boundary layer developed shortly after the surface roughness change.

Schofield (1975) made a significant study in the development of turbulent boundary layer encountering a step change of surface roughness in strong adverse pressure gradient. The velocity profile was found to develop quickly after the

roughness change, the wall shear stress adjusted quickly to the new flow condition with comparatively less overshoot.

Islam (1976) repeated the investigation performed by Carper.Islam and Logan reported that the removal of pressure gradient in the rough channel section did not affect the growth rate of internal boundary layer but the overshooting of the shear stress was reduced.

Toni and Makita (1977) measured mean velocity,turbulence intensities and shear stress in turbulent flow of air in transition from smooth to a rough wall and vice versa in a two dimensional channel. The channel was 1.0 m wide and 10.0cm high. The top and bottom surfaces of the rough section were fitted with 1.5 mmx 1.5 mm cross sectional ribs with pitch of 1.0 cm. Measurements were taken at Reynolds number $3.8x10^4$ based on channel half height and a reference velocity of 10 m/sec. The flow near the wall was found to adjust rapidly to the change in surface roughness, while away from the wall, the response was slow. Adjustment to the new equilibrium condition had set in the internal boundary layer shortly after the roughness change. The shear stress overshoots at the rough smooth junction before returning towards the equilibrium value.

Siuru and Logan (1977) studied the effect of roughness on the turbulent flow through pipe with change in surface roughness condition. They determined the spread of roughness effect from the knee points in the semi-logarithmic plots of mean velocity profiles. The inner layer and the inner sub-layer were distinguished

from the two knee points in the plots. The growth rate of the inner layers was found as $x^{0.5}$

Ali and Islam (1982) investigated the turbulent pipe flow over a zone of step reduction in surface roughness. It was found that the mean turbulent quantities responded immediately to the surface change and needed more length to reach the developed condition than the mean quantities.

Naser (1985) carried out an experiment in an 18 in.X18 in. wind tunnel with 9 ft. long rough section following a 8.5 ft long smooth section. Stone chips of an average size of 0.625 in. was used as roughening elements. It was observed that the flow developed at about a distance of $x/D_t = 5$ from the rough smooth junction. The growth of boundary layer was found to be proportional to $x^{0.4}$. The secondary flow was found to increase with the increase of surface roughness. The wall function was found to be almost proportional to the roughness Reynolds number and almost independent of roughness height.

Uddin (1986) performed the experiment in the same tunnel of Naser (1985) but with a shorter rough section. He carried out the experiment in two roughness orientation, upstanding and depressed. It was observed that the flow was not fully developed even at a distance of $5D_t$ down stream from the smooth rough junction. He observed a sharp drop in axial pressure in the transition zone, indicating high dissipation of flow energy.

CHAPTER-III

GOVERNING DIFFERENTIAL EQUATIONS

3.1 Introduction

Cartesian co-ordinate system is used for the governing differential equation in the present study. The discretized form of the transport equations in cartesian co-ordinate system is simple and the orthogonal grid system makes the computation easier.

In sub-section 3.2.1, co-ordinate free form of the governing equation is presented while in sub-section 3.2.2, the form of the governing equations adequate for use in the present study has been presented in cartesian tensor notation.

When the governing transport equations are time averaged to by pass the prohibitive cost of calculation of the small scale turbulent motion, there appear the unknown Reynolds stress in the mean momentum equation. The modelling of these terms in order to arise at a close set of governing equations is the main task of turbulence modelling. A brief review of the different approaches to this closure problem is given in sub-section 3.3.1. The choice of the closure to be employed in the present study and its underlying assumptions are presented in sub-section 3.3.2.

3.2 Transport Equations

3.2.1 Governing differential equations in General Co-ordinate

The coordinate free form of the equations describing conservation of mass, momentum and scaler quantities can be expressed as:

$$\frac{\partial \rho}{\partial t} + \nabla . (\rho v) = 0 \quad \ldots\ldots\ldots (3.1)$$

$$\frac{\partial (\rho v)}{\partial t} + \nabla . (\rho v \times v - T) = S_v \quad \ldots\ldots\ldots (3.2)$$

$$\frac{\partial (\rho \phi)}{\partial t} + \nabla . (\rho \phi v - q) = S_\phi \quad \ldots\ldots (3.3)$$

Here the density ρ, velocity v and scaler quantity Φ appear as the basic dependent variables. T is the stress tensor, S the source term and q the scaler flux. For a Newtonian fluid the stress tensor can be expressed in terms of basic dependent variables, as:

$$T = -(p + \frac{2}{3}\mu \nabla . v)\, i + 2\mu D \quad \ldots\ldots\ldots (3.4)$$

where p is the pressure, μ the dynamic viscosity, i the unit tensor of the second order and D the deformation or rate of strain tensor. The flux vector is usually given by Fourier type law:

$$q=\lambda\nabla\phi \quad \ldots\ldots\ldots\ldots (3.5)$$

where λ is a proportionality co-efficient, sometimes called "diffusivity" or "conductivity".

3.2.2 The form of governing differential equations adopted for use in this study.

The governing equations for steady incompressible flow are expressed in the general orthogonal cartesian co-ordinate system for this study. The equations are:

$$\frac{\partial}{\partial x_j}(\rho u_j) = 0 \quad \ldots\ldots\ldots\ldots (3.6)$$

$$\frac{\partial}{\partial x_j}(\rho u_i u_j) = -\frac{\partial p}{\partial x_i} + \frac{\partial}{\partial x_j}\left[\mu\left(\frac{\partial u_i}{\partial x_j} + \frac{\partial u_j}{\partial x_i}\right)\right] \quad \ldots\ldots (3.7)$$

$$\frac{\partial}{\partial x_j}(\rho u_j \phi) = \frac{\partial}{\partial x_j}(\Gamma \frac{\partial \phi}{\partial x_j}) + S_\phi \ldots\ldots\ldots (3.8)$$

where u,p, ρ are function of time and the relationship with average value, for example u is obtained as follows (Bradshaw et al 1982).

$$u = \lim (t_1 - t_2) \to \alpha \frac{1}{t_1 - t_2} \int_{t_2}^{t_1} u(x_1, x_2, x_3)\, dt \ldots\ldots\ldots (3.9)$$

similarly, for other variables.

3.3 Turbulence modelling

3.3.1 Introduction

Since "Turbulent fluid motion is an irregular condition of flow in which the various quantities show a random variation with time and space (Hinze, 1977). Therefore, the full Navier - stokes equation are required for an exact mathematical model. However, as is well known, the turbulent velocity fluctuation are characterized by small time and length scales. The governing equations must be solved with appropriately small mesh sizes and time steps to resolve these fluctuations. In the context of present day computer speed and storage capacity, this requirement cannot be satisfied.

To by pass the direct calculations of small scale turbulence, in most engineering applications the predictions of turbulent flows are based mainly on the time

averaged transport equations. The time averaging process consists of expressing each variable through its mean value Φ and fluctuating component Φ' (Schlichiting, 1979), as:

$$\phi=\overline{\Phi}+\phi' \quad \ldots\ldots\ldots\ldots (3.10)$$

If the fluctuations in density and laminar viscosity are assumed to be negligibly small which is usually justified in non-reacting and non-buoyant flows, the decomposition (like equation 3.10) of the dependent variables of equations (3.6), (3.7) and (3.8) into time-averaged and fluctuating components ,gives the following set of equations.

$$\frac{\partial}{\partial x_j}(\rho\overline{u_j}) = 0 \quad \ldots\ldots\ldots\ldots (3.11)$$

$$\frac{\partial}{\partial x_j}(\rho\overline{u_j}\,\overline{u_i}) = \frac{\partial}{\partial x_j}(-\rho\overline{u_j u_i}) - \frac{\partial p}{\partial x_i} + \frac{\partial}{\partial x_j}\left[\mu\frac{\partial \overline{u_i}}{\partial x_j} + \frac{\partial \overline{u_j}}{\partial x_i}\right] + S_i^u \quad \ldots\ldots (3.12)$$

$$\frac{\partial}{\partial x_j}(\rho\overline{u_j}\phi) = \frac{\partial}{\partial x_j}(-\rho\overline{u_j\phi}) + \frac{\partial}{\partial x_j}\left(\frac{\mu}{\sigma_\phi}\frac{\partial \phi}{\partial x_j}\right) + S_\phi \quad \ldots\ldots\ldots (3.13)$$

These equations are similar to their instantaneous counterparts (Eqs.(3.6), (3.7),(3.8)), except for the appearance of the second order co-relations in the momentum and scaler equations,i.e in the former -

$$-\rho\overline{u_i u_j}$$

which represents the turbulent Reynolds stresses; and in the latter there appear the turbulent scaler fluxes:

$$-\rho\overline{u_j \phi}$$

Because of the presence of the turbulent Reynolds stresses and scaler fluxes, the system of equations (Eqs.(3.11),(3.12),(3.13)),do not constitute a close set. Additional equations are therefore required to relate them directly to the mean quantities or determined from their own transport equations. This process of closing the set of equations is known as turbulence modelling.

The available turbulence models are :

(i) Eddy viscosity models

(ii) Reynolds stress model

(iii) Large eddy simulations.

(i) Eddy Viscosity Model

This class of models employ Boussinesq's (1877) concept of eddy viscosity. Here, a Newtonian type of constitutive equation is used between the turbulent stresses and the corresponding mean flow strain rates. For the general Reynolds stress tensor, the Boussinesq's assumption gives:

$$-\rho\overline{u_i u_j}=\mu_t\left(\frac{\partial u_i}{\partial x_j}+\frac{\partial u_j}{\partial x_i}\right)-\frac{2}{3}\delta_{ij}\left(\mu_t\frac{\partial u_k}{\partial x_k}+\rho k\right) \quad \ldots\ldots (3.14)$$

Where μ_t is the eddy viscosity, δ_{ij} ($\delta_{ij} = 1$ for i=j and $\delta_{ij} = 0$ for all other values) is the Kronecker delta and k is the turbulent kinetic energy defined as:

$$k=\frac{1}{2}\overline{u'^2_i} \quad \ldots\ldots\ldots (3.15)$$

Through μ_t, the turbulence viscosity is expressed in terms of quantities which are either known or can be calculated. The most fundamental construction in this regard was Prandtl's (1925) postulation of eddy viscosity, being proportional to the product of a length scale and a velocity scale. The eddy viscosity models differ with respect to the choice and the method of obtaining the respective length and velocity scales.

In "zero-equation" model the turbulent velocity-scale is directly related to the magnitude of mean shear as in Prandtl's (1925) mixing length hypothesis and the length scale is empirically prescribed.

In typical "one-equation" turbulence models, a transport equation for turbulent kinetic energy is solved to obtain the turbulence velocity-scale and the length-scale is prescribed by empirical functions. For example Norris and Reynolds (1975) proposed a "one equation" model for use in the viscous sub-layer as well as in the fully turbulent regions. However "one-equation" models are difficult to be used in the complex shear flows, because the length scale distribution is not easy to prescribe over the whole flow domain (Launder and Spalding [1972]).

In "two-equation" models a transport equation for a length-scale related variable is solved in conjunction with the transport equation for the turbulent kinetic energy,thereby allowing transport effects on the turbulence length-scale to be accounted for. Different workers adopted different length-scale related variables eg. Kolmogorov [1942], Harlow-Nakayama [1968], Jones and Launder [1972], Spalding [1967], Ng-Spalding [1972]. Among these, the rate of turbulence energy dissipation $\varepsilon(=k^{3/2}/l_\varepsilon)$ is favoured partly because of the easy with which its exact transport equations can be derived from the Navier-Stokes equation, and partly of the fact that ε appears directly as an unknown in the equation for turbulent kinetic energy. Reviews of the eddy viscosity models can be found in Launder and Spalding [1972], Bradshaw [1978], and Bradshaw [1981].

(ii) Reynolds Stress Models

These model discard the generalized Boussinesq hypothesis of equation (3.14) and directly employ modelled transport equation for the Reynolds Stress Components.

In the process of deriving these transport equations, higher order co-relations appear as extra unknowns (Reynolds [1976], Rodi [1980] and Gibson [1989]). To close the system of equations at the stress tensor level, the unknown higher co-relations are approximated in terms of other determinable quantities (Rotta [1951], Lumley [1972], Launder et al [1975] and Gibson et al [1981]), resulting in six transport equations, one for each of the stress components. A length-scale equation is also needed, making the total seven equations.

Although the Reynolds Stress Models offer greater potential generality and accuracy, the requirement of solving the above mentioned seven equations make these rank low from the point of view of economy. In addition to being computationally expensive, they sometimes have not proved to be superior to simpler, less expensive models when applied to complex flows (Thompson [1983], El-Tahry [1984]). Further details about Reynolds stress model can be found in (Reynolds [1976], Rodi [1980] and Gibson [1989]).

(iii) Large Eddy Simulation (LES)

This is a completely different line of approach for turbulence modelling. In this method the governing equations are averaged over a spatial volume of the order or larger than the sizes of the computational mesh. Then the dependent variables are replaced by their spatially-averaged and fluctuating components. As a consequence, equations similar to (3.11-3.13) result, but more complicated counterparts of the Reynolds stress terms appear in the equations. However, in

this way motion with scales larger than the mesh sizes can be captured automatically by solving the averaged equations and only the "subgrid" scale motions require modelling. The "subgrid" scale Reynolds stress are modelled, usually using the viscosity concept, as a function of the resolvable scale field. Since the small scales are believed to be more universal in character, they are far more easily modelled than the large scale motions (see for example: Kwak et al [1975] and Clark et al [1979]). The large eddy simulation approach is currently being primarily used to test and develop the time averaged turbulence models described above (Bradshaw [1978], Rody [1988]). Although LES is expensive and still in the developing stage, the promising result already obtained (e.g. Kaned and Leslie, 1983), suggest that it may in due course assume the stature of the main tool for engineering analysis.

3.3.2 Turbulence Model for the Present Study

Despite the greater potential of the Reynolds stress models the over riding demands of economy nominates the standard K-ε model (Launder and Spalding 1972) in which the unknown Reynolds stress are expressed by means of gradient transport hypothesis where the fluxes are assumed proportional to the gradients of mean flow properties. The constant of proportionality is μ_t.

According to gradient transport hypothesis (Hinge [1959]).

Reynolds Stress:

$$-\rho\overline{u_i u_j} = \mu_t \left(\frac{\partial u_i}{\partial x_j} + \frac{\partial u_j}{\partial x_i} \right) \quad \ldots\ldots\ldots (3.16)$$

μ_t turns out to be a function of turbulence energy k and its dissipation rate ε via $\mu_t = c_\mu \rho k^2/\varepsilon$ where k and ε are derived from their own transport equations.

For steady turbulent flow, the modelled form of the k - equation and ε - equations used in the present study are:

k-equation

$$\frac{\partial}{\partial x_j}(\rho u_j k) = \frac{\partial}{\partial x_j}\left(\frac{\mu_{eff}}{\sigma_k} \frac{\partial k}{\partial x_j} \right) + G - \rho\epsilon \quad \ldots\ldots\ldots (3.17)$$

ε- equation

$$\frac{\partial}{\partial x_j}(\rho u_j \epsilon) = \frac{\partial}{\partial x_j}\left(\frac{\mu_{eff}}{\sigma_\epsilon} \frac{\partial \epsilon}{\partial x_j} \right) + C_{\epsilon_1} \frac{\epsilon}{k} G - C_{\epsilon_2} \rho \frac{\epsilon^2}{k} \quad \ldots\ldots\ldots (3.18)$$

Where G is the rate of production of turbulent kinetic energy defined as:

$$G = \mu_t \left(\frac{\partial u_i}{\partial x_j} + \frac{\partial u_j}{\partial x_i} \right) \frac{\partial u_i}{\partial x_j} \quad \ldots\ldots (3.19)$$

For two dimensional steady plane flow, the equation (3.19) can be written as:

$$G = \mu_t \left[2 \left(\frac{\partial u}{\partial x} \right)^2 + 2 \left(\frac{\partial v}{\partial y} \right)^2 + \left(\frac{\partial u}{\partial y} + \frac{\partial v}{\partial x} \right)^2 \right] + S_G \quad \ldots\ldots\ldots (3.20)$$

Where, S_G covers additional generation term whose effects are small except for flows of non-uniform properties. For present prediction this term is omitted and S_G given by (ideriah [1975]).

Where $\mu_{eff} = \mu + \mu_t$

$$S_G = -\frac{2}{3}\mu_t\left(\frac{\partial v}{\partial y}+\frac{\partial u}{\partial x}\right)^2 \ldots\ldots\ldots (3.21)$$

The values of the empirical constants (C_μ, $C_{\varepsilon 1}$, $C_{\varepsilon 2}$, σ_k, σ_ε) used in the study taken from Launder & Spalding [1974] and given in table 3.1.

Table 3.1: The values of empirical co-efficient in the k-ε model

C_μ	$C_{\varepsilon 1}$	$C_{\varepsilon 2}$	σ_k	σ_ε
0.09	1.44	1.92	1.0	1.3

Near wall region

In the standard high Reynolds number k-ε model, the steep gradients prevailing in the viscosity affected near wall region are not resolved in the Numerical Calculations; rather they are past by placing the first grid point away from the wall and outside the viscous sub-layer, where the flow is sufficiently turbulent and the velocity is linked to the wall shear stress by the logarithmic law of the wall. In the derivation of the logarithmic velocity distribution law, it is assumed that: (i) the shear stress across the layer is constant; (ii) the length scale increases linearly with the distance from the wall such that $l_\varepsilon \alpha$ ky and (iii) the rate of production (G) of turbulence energy balances its rate of dissipation, ε. Under the couette flow condition, the log law is given by:

$$\frac{u}{u_\tau} = \frac{1}{k} \ln y + A \ldots\ldots\ldots (3.22)$$

Where A is a function of the wall roughness, u_τ the friction velocity defined as $u_\tau = (\tau_w/\rho)^{0.5}$ where τ_w is the wall shear stress and K is known as von kerman constant (K=0.4187).

CHAPTER-IV

NUMERICAL SOLUTION

4.1 Introduction

In this chapter the numerical solution procedure of the governing differential equations presented in the previous chapter is described.

In section 4.2, the governing equations for two dimensional problems are written in the expanded form suitable for discretisation.

In section 4.4, the differencing schemes used to evaluate various terms (convection, diffusion and source terms) are discussed from the point of view of numerical stability, accuracy and economy and accordingly a choice is made for the present study.

Section 4.5 describes the overall solution procedure.First the grid and variable arrangement used are presented then the pressure correction equation which links the momentum and continuity, is described.The treatment of the boundary condition is discussed next. Finally, the solution algorithm is presented.

4.2 Expanded Form of Governing Differential Equations

For the sake of easier manipulation, the compact forms of the governing differential equations (given in the previous chapter) are rewritten here for steady two dimensional case as

continuity equation:

$$\frac{\partial}{\partial x}(\rho u) + \frac{\partial}{\partial y}(\rho v) = 0 \quad \ldots\ldots\ldots\ldots\ldots\ldots (4.1)$$

u-momentum equation:

$$\frac{\partial}{\partial x}(\rho u^2) + \frac{\partial}{\partial y}(\rho uv) = -\frac{\partial p}{\partial x} + \mu_{eff}\left(\frac{\partial^2 u}{\partial x^2} + \frac{\partial^2 u}{\partial y^2}\right) \quad \ldots\ldots\ldots (4.2)$$

v-momentum equation:

$$\frac{\partial}{\partial x}(\rho uv) + \frac{\partial}{\partial y}(\rho v^2) = -\frac{\partial p}{\partial y} + \mu_{eff}\left(\frac{\partial^2 v}{\partial x^2} + \frac{\partial^2 v}{\partial y^2}\right) \quad \ldots\ldots\ldots\ldots (4.3)$$

General differential equation:

$$\frac{\partial}{\partial x}\left(\rho u\phi - \Gamma_\phi \frac{\partial \phi}{\partial x}\right) + \frac{\partial}{\partial y}\left(\rho v\phi - \Gamma_\phi \frac{\partial \phi}{\partial y}\right) = S_\phi \quad \ldots\ldots (4.4)$$

4.3 The method of discretization

The governing differential equations can be discretized in many ways. An over view of the discretization method for the numerical solution of the fluid flow

problems is given by PATANKAR (1980). In the present study the finite volume approach, as described by Gosman et al (1969) and others, is adopted. In this approach, the governing differential equations are discretized by integrating them over a finite number of control volumes or computational cells, into which the solution domain are divided. A typical computational cell is shown in Fig. 3.1. Typical discretized transport equation (e.g. eq. 4.4) will take the following quasilinear form.

$$(a_p - b)\,\phi_p = \sum a_{nb}\phi_{nb} + c \quad \ldots\ldots\ldots (4.5)$$

Where, the a_{nb} are coefficients multiplying the values of Φ at the neighbouring nodes surrounding the central node P. The number of neighbour depends on the interpolation practice or differencing scheme used. The a_{nb} contains combined convection and diffusion contribution at the control volume faces, i.e.

$$a_{nb} = a_{nb}^{C} + a_{nb}^{D} \quad \ldots\ldots\ldots (4.6)$$

a_p is the coefficient of Φ_p given by:

$$a_p = \sum a_{nb} \quad \ldots\ldots\ldots (4.7)$$

and b and c are obtained by linearizing the source term as follows.

The source term (right hand terms of the eqn. 4.4.) are evaluated by integrating the volumetric source s_ϕ over the volume of the computational cell and expressed as:

$$-\int_v s_\phi dv = b\phi_p + c$$

where, c stands for the constant part of the source term while b is the coefficient of Φ_p and often a function of Φ_p.

Since the direct solution methods (i.e. matrix inversion) require very large computer storage and time and since the governing transport equations are non linear, (the discretised governing transport equations are seemingly linear but a_p being the function of Φ_p makes them virtually nonlinear) the discretised equations are solved using the SIMPLE algorithm of Patanker and Spalding [1972] by repeated sweeps of a line-by-line application of the Tri-Diagonal Matrix Algorithm (TDMA) (Patanker [1980]).

4.4 Differencing Scheme

4.4.1 Choice of Differencing Schemes

The stability of the numerical algorithm and the accuracy of the solution obtained both depend on the type of interpolation practices or differencing schemes used. The solution of the discretized equations (4.5) should satisfy the following important properties of the exact solution:

(i) The flux that leaves a cell through a particular cell must be identical to the flux that enters the next cell through their common face.

(ii) The conservation principle must be ensured i.e. the net transport of Φ across the solution domain boundaries should equal total production or consumption by integral sources.

(iii) The co-efficient of resulting algebraic equations must be always of the same sign, to ensure diagonal dominance of the co-efficient matrix (i.e.when the matrix of the coefficients of these equations is written, all the non zero coefficients align themselves along three diagonals of the matrix).

(iv) The sources must be treated in a special manner. So as to reduce the occurrence of unbounded solutions of problems which are source dominated. In general the source should be linearized with a negative slope, to avoid violation of rule above (see Patankar [1972]).

(v) To be consistent with the differential equation, the co-efficient a_p must obey the relation given by equation (4.7) in the absence of source and boundary conditions.

(vi) Since all iterative schemes are prone to divergence, the finite difference equations must obey certain criteria to ensure convergence.

The Scarborough criteria is one such rule. A sufficient condition for convergence is that

$$\frac{\sum |a_{nb}|}{|a_p|} \leq 1, \quad \textit{for all equations}$$

and < 1 for at least one equation.

These are basic desired properties expected of a differencing scheme. The optimum differencing schemes must be stable and highly efficient.

4.4.2 Brief Review of Some Differencing Schemes

In this subsection the differencing schemes used to evaluate convected cell-face value of the dependent variable in terms of surrounding nodal values are discussed and final choice is made for the present study.

(i) **Central differencing schemes (CDS):** If a piece wise-linear profile of Φ is assumed between P and E (see Fig. 3.6), the cell face value Φ_e is given by:

$$\phi_e = \phi_E f_p + \phi_p (1 - f_p) \quad \ldots\ldots (4.8)$$

where f_p is a linear interpolation factor defined as:

$$f_P = \frac{\Delta x_P}{\Delta x_P + \Delta x_E}$$

Here ΔX_P and ΔX_E are the cell dimensions along x coordinate for P and E cells (see Fig. 3.1 and 3.6).

In this scheme a_E and a_N are always negative and if the convection process dominates this can cause the whole coefficient a_{nb} to assume negative value. As a result the scarborough criteria fails and produce unbounded solutions (Spalding [1972], Rathby & Torrance [1974]). At high Peclet number the CDS also violates the transportive property by employing downstream nodes in expressions given above. For these reasons application of CDS is limited to low Reynolds number problems.

(ii) **Upwind differencing scheme (UDS)**: The upwind differencing scheme (Runchal & Wolfshtein [1969]) recognizes that the weak point in the preliminary formulation is the assumption that the convected property Φ_e at the interface is the average of Φ_E and Φ_P and it propose a better prescription. The formulation of the diffusion term is left unchanged but the convention term is calculated from the following assumption.

The value of Φ at an interface (See Fig. 3.7) is equal to the value of Φ at the grid point of the upwind side of the faces.

Thus $\Phi_e = \Phi_P$ if $f_e > 0$

$$= \Phi_E \text{ if } f_e < 0$$

In this scheme all the coefficients contributing to a_p are always non-negative. As a result Scarborough criteria is satisfied. UDS also satisfies the property of transportiveness, and thus the boundedness of the solution is guaranteed.

In terms of Taylor Series Truncation Error (TSTE) analysis, the UDS is first order approximate.

If the flow direction is not aligned with one set of grid lines and if there is a steep gradient of dependent variables in the direction normal to the flow, the use of UDS results severe numerical smearing, as if much stronger diffusion process were present in the flow than actually is the case, this additional diffusion is called the "false" diffusion. It is zero if angle between flow and grid lines is 0° or 90° and maximum when 45°. "False" diffusion originates from the fact that interpolation is performed along the grid lines rather than the streamlines. The question of false diffusion attains importance only in case of large Peclet numbers, since at small peclet numbers, the real diffusion is relatively large (see for detailed discussion Patanker [1980] and Lai [1982]).

(iii) **<u>Linear upwind differencing scheme (LUDS):</u>** In the Linear upwind differencing scheme the convected cell-face values are obtained by linear extrapolation from the two closest upstream neighbour nodes on the same coordinate line (See Figure 3.8).

$$\Phi_e = \Phi_P + (\Phi_P - \Phi_W)\,(1-f_W); \text{ for } f_e > 0$$

$$= \Phi_E + (\Phi_E - \Phi_{EE})f_E \qquad \text{for } f_e < 0$$

In this scheme negative coefficients appear at the distant nodes violating the Scarborough criteria. However, the LUDS does satisfy both the properties of conservativeness and transportiveness and in terms of TSTE it is second order accurate; hence unless boundedness problems arise the LUDS can produce much higher level of accuracy than the UDS under the same circumstances.

Among the other available schemes are the Skew upwind differencing scheme (SUDS) (Rathby [1976]) and Quadratic upwind differencing scheme (QUDS) (Leonard [1979]).

SUDS suffers less from the numerical diffusion problem but is considerably more complex. The QUDS is suitable for implementation in general two-dimensional applications but is computationally more expensive than LUDS; and LUDS is more suitable for iterative solution methods (Peric [1985]).

For the present study the UDS has been adopted.

4.5 Solution Procedure

4.5.1 Grid & Variable Arrangement

In the present study, the numerical solution is accomplished on a variably spaced staggered mesh [see for example Caretto et al (1972), Patankar (1980)], in which the scaler quantities (including pressure, density, viscosity, k & ε) are defined at the centre and the normal velocities at cell faces, as shown in Fig. 3.5. It has the advantage that the variables u,v, p are stored such that the pressure gradients which drive the velocities u & v are easy to evaluate and moreover the velocities are located where they are needed for the calculation of convective flux.

4.5.2 Calculation of Pressure

The pressure gradient forming part of the source term in the momentum equations are to be obtained before the velocity field is calculated and it is the pressure field through which the continuity equation is satisfied.

The SIMPLE method of Patanker and spalding [1972] is used in the present study to obtain pressure. The differential equations presented in section 4.2 can be expressed in the following discretised form.

$$[(\rho U)_e - (\rho U)_w]\Delta y + [(\rho V)_n - (\rho V)_s]\Delta x = 0 \quad \ldots\ldots (4.9)$$

$$a_e u_e = \sum a_{nb} u_{nb} + b + (p_P - p_E) A_e \quad \ldots\ldots\ldots\ldots (4.10)$$

$$a_n V_n = \sum (a_{nb} V_{nb}) + b + (P_p - P_N) A_n \quad \ldots\ldots (4.11)$$

$$(a_p - b)\phi_p = \sum a_{nb}\phi_{nb} + C \quad \ldots (4.12)$$

The solution method consists of following stages

A guessed pressure field p^* is used to obtain a preliminary set of U and V from the following equations

$$a_e u_e^* = \sum a_{nb} u_{nb}^* + b + (p_P^* - p_E^*) A_e \quad \ldots\ldots\ldots (4.13)$$

$$a_n V_n * = \sum a_{nb} V_{nb} * + b + (P_p * - P_N *) A_n \quad \ldots\ldots (4.14)$$

where, the superscript * on U and V indicates that these are based on an estimated pressure field p_*.

The starred velocity U^* and V^* will in general not satisfy the continuity equation (4.9) but will produce a net mass source M_p for the point P. This is defined by

$$M_p = [(\rho U^*)_e - (\rho U^*)_w]\,\Delta y + [(\rho V^*)_n - (\rho V^*)_s]\,\Delta x \quad \ldots (4.15)$$

Now our aim is to correct the pressure and velocity so as to eliminate this mass source: For this, let us propose that a corrected value P is obtained from the following equations.

$$p = p_* + p'$$

where, p' is called the pressure correction. The corresponding velocity corrections u' and v' are obtained, in similar manner as:

$$u_e = u_{e*} + u'$$

$$V_n = V_n^* + V$$

substituting 4.13 from 4.10 we have

$$a_e u'_e = \Sigma a_{nb} u'_{nb} + (p'_P - p'_E) A_e \quad \ldots\ldots\ldots (4.16)$$

Dropping the term $\Sigma a_{nb} u'_{nb}$ from the above equation for computational convenience, equation (4.16) becomes

$$a_e u'_e = (p'_P - p'_E) A_e$$

$$\acute{u}_e = d_e(\acute{p}_P - \acute{p}_E) \text{ , where , } d_e = \frac{A_e}{a_e}$$

Equation 4.16 is the velocity correction. Hence the corrected velocity equations becomes

$$u_e = u_e^* + d_e(P_p' - P_E') \text{ . . . . . (4.17)}$$

Similarly we can write

$$V_n = V_n^* + d_n(P_p' - P_N') \text{ . . . . (4.18)}$$

Substituting the above velocity correction equations (4.17 and 4.18) into continuity equations (4.9), we have discretised equations for P′

$$a_p P_p' = a_E P_E' + a_w P_w' + a_N P_N' + a_s P_s' + b \text{ . . . . (4.19)}$$

4.6 Boundary Conditions

The forms of boundary conditions encountered in the present study and their implementations are described below

(i) Inlet boundaries: The values of all the variables at the inlet boundaries are usually explicitly specified, from experimental data, or are obtained from analysis and estimation.

(ii) Outlet Boundaries: At outlet of the computation domain at large Re, upwind difference renders specifications of variables unimportant (in the absence of recirculation). It is usual practice to assume zero gradient in the direction of flow and the exit velocities are obtained from mass balance.

(iii) Impermeable Wall: Near the wall the local Reynolds number becomes very small and the turbulence model applicable at high Reynolds number becomes inadequate. Both the fact and the steep variation of properties near the wall necessitates special attention for the grid nodes close to walls.

4.6.1 On the basis of wall boundary conditions

Wall boundary conditions are embodied in the governing transport equations in the following ways:

(a) Equations of Mean Motion

At the solid walls the velocities are set to zero, satisfying the no slip condition. The boundary layer that develops near the wall can be conceived to be made up of three zones (Hinze [1959]).

$Y^+ < 5$ viscous sub layer

$5 < Y^+ < 30$ buffer layer

$30 < Y^+$ internal layer

defined according to the dimensionless distance Y^+ given by $Y^+ = \rho\, u_\tau\, y / \mu$

Where y is the normal distance from the wall and u_τ is the friction velocity defined as $u_\tau = (\tau_w / \rho)^{0.5}$ here τ_w is the wall share stress.

Generally close to the wall, a one dimensional cuette flow analysis is made and the momentum equation can be reduced to a particularly simple non dimensional form as follows (Gosman et al 1978).

$$\tau = (\mu + \mu_t)\frac{du}{dy}$$

$$\tau_w = \left(1 + \frac{\mu_t}{\mu}\right)\frac{du^+}{dy^+}$$

$$For, y^+ \leq 11.63; \frac{\mu_t}{\mu} \ll 1, \tau \approx \tau_w, then, u^+ = y^+$$

$$For, y^{+}>11.63; \frac{\mu_t}{\mu} \gg 1, \tau \approx \tau_w$$

and $\mu = \rho\ k\ y\ \mu_\tau$ (Hinze, 1959)

then $u^{+} = 1/k \log_e (Ey^{+})$

where $u^{+} = u/u_\tau$

K = von kerman constant (0.4187)

E = integral constant

In the standard k- ε model (Launder and Spalding, 1972) the wall affected region is bridged by logarithmic law of the wall.

(b) Equations of Turbulence Energy and Energy Dissipation

The wall treatment for k- and ε - equations are to be formulated on the basis of local equilibrium condition that the local rete of production of turbulence is balanced by its dissipation rate ε.

(1) The turbulence energy equation (eq.3.17) reduces to a simple form that yields expression for both the shear stress $\tau = \tau_w$ and the dissipation rate ε within the buffer and viscous sub-layer

production = dissipation

$$thus, -\overline{uv}\frac{du}{dy} = \epsilon : yielding, k = \frac{\tau}{\rho c_\mu^{\frac{1}{2}}}$$

and the ε modified from the k balance as

$$\int_v \epsilon dv = c_\mu^{\frac{3}{4}} k^{\frac{1}{2}} u^+ \frac{dv}{y_p}, with$$

$$u^+ = y^+, for, y^+ \leq 11.63$$

$$u^+ = \frac{1}{k}\log_e(Ey^+) ; for, y^+ > 11.63$$

(ii) ε equation reduces to

$$c_{\epsilon_1} = c_{\epsilon_2} - \frac{k^2}{\sigma_\epsilon c_\mu^{\frac{1}{4}}}$$

$$thus, \sigma_\epsilon = \frac{k^2}{(c_{\epsilon_1} - c_{\epsilon_2})\, c_\mu^{\frac{1}{4}}}$$

4.6.2 Incorporation of wall boundary condition

(a) Momentum equation

(i) Tangential velocity:

Tangential velocity u_p for a node next to the wall as shown in Fig. 3.9 is obtained from usual momentum balance and the coefficient a_s is set to zero in the finite difference equation. The correct shear force expression is incorporated via source treatment. The momentum source for tangential velocity component adjacent to the south wall is calculated as

$$S_s=\tau_s\delta x_{ew} = \mu_{eff}\delta x_{ew}(u_p-u_s)/y_p$$

where δx_{ew} is the area of cell ,y_p is the normal distance from cell centre to the wall and μ_{eff} is the effective viscosity,can be expressed as

$$\mu_{eff}=\mu \; ; for, y^+ \leq 11.63$$

$$\mu_{eff}=\rho c_\mu^{\frac{1}{4}} k_{pw}^{\frac{1}{2}} k \frac{y_p}{\log(Ey_p^+)} \; ; for, y^+ > 11.63$$

$$with, y_p^+ = c_\mu^{\frac{1}{4}} \rho_p k_{pw}^{\frac{1}{2}} \frac{y_p}{\mu}$$

where $k_{pw} = (k_p + k_w)/2$

S_s is then linearized as equation $S=S_u+S_p\Phi_p$ where S_p and S_u represent the implicit and explicit contribution respectively.

$S_p = \mu_{eff}\delta x_{ew}/yp$

$Su = \mu_{eff}\, u_s\, \delta x_{ew}/y_p$

(ii) Normal velocity: For velocity normal to a wall ,no special wall treatment is necessary.

(b) Turbulence Energy K

Kp shown in fig 3.10 is obtained from usual k-balance but, since the turbulence energy falls to zero at the wall, there is no contributing flux from the wall: hence, a_s is set to zero without insertion of any modified form for it. The generation term G in the K-equation reduces to a much simplified form which is further modified by noting that it can be expressed in terms of wall shear stress. The source for the K-balance, $s_k = (G-\rho\varepsilon)$, is evaluate as follows.

(i) Calculation of G altered by noting

and $\tau_s = \mu_{eff}\,(U_p - U_s)/\, Y_p$

$$\int_v \mu_t \left(\frac{\partial u}{\partial x} + \frac{\partial v}{\partial y} \right)^2 dv \approx \tau_s (u_p - u_s) \frac{\partial v}{y_p}$$

(ii) Calculation of $\rho\varepsilon$ altered by noting

$$\int_v \rho \epsilon dv \approx \rho c_\mu^{\frac{3}{4}} \left(k_p^{\frac{3}{2}} - k_s^{\frac{3}{2}} \right) u^+ \frac{\partial v}{y_p}$$

$u^+ = y^+$ for $y^+ < 11.63$

$= 1/k \log_e (Ey^+)$ for $y^+ > 11.63$.

(c) Energy Dissipation Rate ε

In wall-flows, unlike k which falls to zero at the wall, ε reaches its highest value (much higher than in a free stream) at the wall. This makes ε-balance for a cell extending upto a wall very difficult as we are ignorant on how to modify a_s in such cases. It is due to this shear ignorance that we adopt a fixed value for ε_p (irrespective of y_+) based on `equilibrium' relation. ε_p is incorporated as usual through way of b and c.

$$\epsilon_p = c_\mu^{\frac{3}{4}} k_p^{\frac{3}{2}} / k y_p$$

(d) Pressure Correction

At boundaries where the normal velocity is prescribed, the finite difference equation for local pressure correction must be defined so that this velocity is not

changed i.e. p/ is zero. This is done, for example the cell adjacent to a 'south' wall by setting as = 0.

4.7 Solution Algorithm

Now the important operation in the order of their execution are

(i) Initialise all field values by an initial guess

(ii) Solve momentum equations and obtain u^* and v^*

(iii) Solve the pressure correction equation to obtain p' and calculate p by adding p' to p^*

(iv) Calculate u, v from their starred values using velocity correction formula

(v) Solve the discretized equation for other variables (such as turbulent quantities) If they influence the flow field through fluid properties, source terms etc.

(vi) Treat the corrected pressure p as a new guessed pressure p*, return to step (ii) and repeat the whole procedure until a converged solution is obtained.

In the present study, the convergence criterion is that the sum of the normalized absolute residuals at all computational nodes, defined

$$R_\phi{}^r = \sum_N | (a_p^r - b^{(r-1)}) \phi_p^{(r-1)} - \sum a_{nb}^r \phi_{nb}^{(r-1)} - c^{(r-1)} | / N_f$$

should fall below a specified level

$R_\phi{}^r < 10^{-3}$

Here N is the total number of nodes, r the iteration counter and N_f the normalization factor.

CHAPTER-V

PRESENTATION OF RESULTS AND COMPARISON WITH EXPERIMENT

5.1 Introduction

In this chapter, the results of the numerical prediction of turbulent flow over smooth to rough surface obtained by the numerical method described in Chapter-4 are presented and compared with the measurements of Naser [1985]. To simulate the same rough surface used in the experiment by Naser [1985] two different types of roughness configuration are employed in the calculation domain i.e. (i) uniform plain surface with step up height equal to roughness height 1.59 cm (average roughness height used in the experiment), (ii) saw tooth type rough surface with tooth height 1.59 cm (average roughness height used in the experiment) Standard k-ε model incorporated with upwind differencing scheme is used in the computation. Analysis of the flow structure is carried out at four different Reynolds numbers (Reynolds number is defined as $Re = \rho U D_t/\mu$, where ρ is the density of the fluid, U is the axial centre line velocity of the flow, D_t is the width of the test section and μ is the dynamic viscosity of the fluid). Effects of the different roughness configuration on the computational flow field are presented. Turbulence energy and energy dissipation rate are presented for clear understanding of flow development at different Reynolds numbers.

5.2 Flow Configuration

The steady and incompressible turbulent flow geometry considered here was the subject of a detailed experimental investigation performed by Naser [1985]. The geometry and dimension of the test section is shown in Fig.1. The flow measurements were performed for four different Reynolds number over the smooth to rough surface with average stone chips of hight 1.59 cm. The effect of the side walls on the core region of the flow, specially the two-dimensional vertical plane passing through the centre line, was found to be negligible (Naser [1985]). Hence calculation were carried out on a two dimensional plane representing a vertical plane passing through the centre line of the duct. The surface texture of rough portion used in the experiment, is simulated in the present computations in two different ways i.e. (i) on the bottom surface of the calculation domain five cells of total height of 1.59 cm (equal to the height of the average stone chips used in the experiment to make rough surface) are blocked off to incorporate the rough surface into the flow domain at a distance of 2.59m from the inlet; (ii) on the bottom surface, at a distance of 2.59m from the inlet, cells are blocked off in such a way that the blocked cells give the bottom surface a shape of saw tooth type configuration with the maximum saw tooth height 1.59 cm.

5.3 Domain of Solution and Computational Grid

The solution domain shown in Fig.2(a) & Fig.2(b) is bounded by the inlet plane, exit plane and the top and bottom wall. The entire computational domain is

divided into 50 vertical grid lines and 144 horizontal grid lines. The grid distribution in the calculation domain is uniform in the x-direction (horizontal) and non uniform in the y-direction (vertical). The mesh is contracted near the bottom all over the whole calculation domain such that the ratio between the two successive steps in space is constant and equal to 1.15.

5.4 Boundary Conditions

The treatments of the walls, the inlet and the outlet applied in the present study has already been presented in Section 4.6. In the following, the specification of the boundary values at the inlet form the experimental data are outlined and finally the treatment of the exit boundary is described.

5.4.1 Inlet Conditions

The uniform velocity distributions across the inlet section were obtained from the measured mass flow rates of Naser [1985]. Turbulent energy and energy dissipation rates are calculated from the following formula.

$$K = 0.03u^2 \quad \ldots\ldots\ldots (5.1)$$

$$\epsilon = \frac{k^{\frac{3}{2}}}{.09 l_\epsilon} \quad \ldots\ldots\ldots (5.2)$$

5.4.2 Outlet Condition

It is already outlined in section 4.6 that, in the absence of recirculation and at large Reynolds numbers, specification of variables at the outlet of the calculation domain is obtained by assuming a zero gradient in the flow direction.

5.5 Grid Dependence Test

To obtained a solution independent of the number and spacing of the grid nodes, grid dependence test is performed. The test was done at Reynolds numbers 2.127 X 10^5 for two grid sizes: 30 X 50 and 50 X 72, for smooth surface. Each time close spacing was maintain at the bottom wall, where rapid changes of the flow variables occur. For this test, predicted u-velocity profiles at various axial location was compared with measured values of Naser [1985]. The predictions for both the grid sizes are in close agreement with the measurements and hence the solution is independent for any grid sizes.

5.6 Presentation of Results and Comparison with Experiment

The flow parameters are presented here with the duct hydraulic diameter (D_t) as the characteristic length.The centre line velocity at each section of the duct has been taken as characteristic velocity.

The mean flow characteristics has been calculated at four different Reynolds numbers viz. Re=2.127×10^5, 5.76×10^5, 7.98×10^5, 9.57×10^5 based on the hydraulic diameter of the duct and mean centre line axial velocity over the smooth surface. The calculations and comparisons include mean axial velocity profiles, pressure gradient along the wall, wall shear stress and log-law parameters.

Mean Velocity Profile

The mean velocity profiles of flow over the smooth surface for different Reynolds numbers are shown in Fig 4.1 along with the experimental results. The mean velocity profile over the entire diameter of the duct for smooth surface at a distance x/D_t=-0.83, (x measured from smooth rough junction) at Reynolds number 5.76×10^5 is plotted in Fig. 4.2. The vertical distances for the velocity profiles are calculated from the smooth wall. The velocity profiles are in quite good agreement with the experimental values and indicate the attainment of self- preservation characteristics. However, some disagreements are observed at the top of the boundary layer, where the computational result under predicts the velocity. This disagreement is more pronounced at the highest Reynolds number (9.57×10^5), where the maximum deviation is 4.0%.

The mean axial velocity profiles, calculated over the rough surface using two types of rough texture, are shown in Fig. 4.3 along with the experimental results. The vertical distances for velocity profiles are calculated from the top of the rough surface. The velocities are non-dimensionalised by the free stream velocity of the

respective sections and distances are by the duct diameter. The profiles show a gradual development of boundary layer with axial distance and the trend indicates that the flow attains development at x/D_t=5.5. The computational results obtained with mean-height rough texture are in reasonably good agreement with the experimental data,whereas the results obtained with saw-tooth rough texture are in good agreement only at the smooth-rough junction (x/D_t=0.0), but gradually deviates further from the experimental values in the down stream direction. This discrepancy reaches at its maximum at x/D_t=5.5. At x/D_t=5.5, the experiment and the mean-height results show that the boundary layer is developed, whereas the saw-tooth results show a developing trend.

Axial Pressure Gradient

The distribution of wall static pressure in the axial direction are shown in Fig. 4.4 along with experimental data. The curves show three distinct regions, the first straight line portion represents the smooth wall pressure gradient. The second portion shows a sudden jump followed by a sharp decrease in the transition zone associated with the accelerated flow. The sharp decrease is due to the sudden decrease in flow area by the presence of roughness configuration. After a certain distance downstream, the pressure gradient takes a new equilibrium value for the rough surface. In the equilibrium zone of the rough surface the slope of the pressure gradient curve is much higher than that for the smooth section. This is due to higher frictional and other resistances.

The predictions show good agreement with the measurements of Naser [1985] in the smooth section but discrepancies are evident in the rough sections. In the saw-tooth type rough surface the discrepancies are within the acceptable range but in the mean-height type rough surface, pressure gradients are highly under predicted. This is due to the fact that mean-height type rough surface under predicts the shear stress.

Friction Factor

The wall shear stress presented in the form of friction factor for the smooth surface is determined from the axial pressure gradient in the smooth section of the duct. If the wall shear stress is assumed to be uniform throughout the perimeter of the duct, then the simple force balance provides.

$$\tau_{0s} = \left(\frac{dp}{dx}\right)_s \frac{D_t}{2} \quad \ldots\ldots 5.3$$

The friction co-officiants obtained from the relation

$$c_f = \frac{2\tau_{0s}}{\rho u^2} \quad \ldots\ldots (5.4)$$

are plotted in Fig. 4.5 along with the measurement of Naser [1985] and other researchers. The predicted friction co-efficients for smooth surface are in good agreement with the measurements.

The method of calculation of shear stress and friction coefficient is followed from the experimental study of Naser [1985].

The friction co-efficient calculated for two types of rough surfaces are plotted in Fig. 4.6 along with those of other researchers. The curves show a sharp difference between the friction co-efficient obtained by saw tooth type rough surface and mean height type rough surfaces. This is due to the fact that the pressure gradient for saw tooth type rough surface is much higher, conforming with the experiment. Whereas for the mean height type, the pressure gradient is much lower than that obtained in the experiment. This is already explained earlier with reference to Fig. 4.6.

The predicted friction co-efficient for saw tooth type rough surface is in good agrement with the measured data whereas, high discrepancy is evident for the mean height type rough surface.

Log-Law Profiles

The universal velocity profiles over the smooth surface are shown in Fig. 4.7. along with the measured data of Naser (1985). The mean velocity and the wall distance

are normalised by $u^* [(\tau_o/\rho)^{.5}]$ and ν/u^* respectively. The straight line nature and parallelism of the two profiles (x/D_t = -1.167, - 0.25) show that the flow is developed before meeting the rough surface. The logarithmic velocity profiles for the rough surfaces are shown in Fig. 4.8a and 4.8b for Reynolds number Re = 9.57 X 10^5 at x/D_t = 5.5 along with experimental values. The nature of the curves show that the flow is almost developed. The log low profiles for the rough surface shows a vertical shift from the smooth wall profiles for the same Reynolds number flow. This is termed as the "wall function" of the rough surface and are found to increase with the roughness Reyonlds number ku^*/υ.

The log-law profiles for smooth surface conforms with the experimental data. But the predicted values for rough surface deviate from the measured data. The deviation from measured data for saw tooth type rough surface is due to the fact that the mean velocity profile for saw tooth type rough surface does not conform with the experimental data, and for mean height type rough surface, pressure gradient is highly under predicted.

5.7 Discussion

Two dimensional steady incompressible flow has been simulated for the prediction of turbulent boundary layer in transition from smooth to rough surface. The results obtained have been presented in the previous section. Standard k - ε model incorporated with upwind differencing scheme has been used for the calculation of flow characteristics. The simulation of rough surface has been carried out in two

different ways mentioned in previous section. The predications of flow field for smooth surface are in quite good agreement with the measured data. However, the disagreements which are still there, may be due to the fact that the grids considered for finite-difference solution has not been sufficient enough to resolve the gradients of the flow parameters to reveal all the minute details of the flow field.

But the predicted flow characteristics for rough surface indicate discrepancies with the measured data. It may be mentioned here, that the rough surface used for computation are of two different geometrical configurations, namely (i) regular saw tooth type and (ii) mean height type. The discrepancies between the predicted and measured data may be due to the following reasons;

- None of the two rough models represents the exact rough surface created by randomly organised irregular stone chips used in the experiment.

- The randomly oriented irregular stone chips used in the experiment disperse the flow in an irregular fashion. This could not be incorporated and simulated in the flow calculation.

- The irregular stone chips used in the experiment, redistributes the flow in the three-dimensional space whereas the regular saw tooth type rough texture merely gives the two-dimensional effect of the roughness elements.

- In the experiment small vortices are formed in between the stone chips. Energy required to drive these small vortices are obtained form the mean flow, resulting in higher shear stress. This could not be reproduced in the calculation.

- Mean height types simulation may be considered as smooth surface with a jump; but the experimental rough surface has been quite different from the assumed system.

- In the rough section, where the steep pressure gradients and the minute details of the flow near the solid wall influences the over all flow characteristics. k-ε model is inadequate for satisfactory simulation.

- In the derivation of the logarithmic velocity distribution law, it is assumed that

  (a) Shear stress across the layer is constant.

  (b) The length scale increases linearly with the distance from the wall.

  (c) The rate of production of turbulent energy balances its rate of dissipation.

None of the above mentioned assumptions are valid in the near rough wall region.

- Computer storage limitations restricts the use of fine meshes in the calculation domain.

- All the desirable characteristics contributing to numerical accuracy can not be maintained simultaneously throughout the whole calculation domain due to complex geometry of rough texture.

If all the above mentioned limitations are overcome, then the computation will reproduce the results obtained by the measurements.

CHAPTER-VI

SUMMARY AND CONCLUSIONS

6.1 General

In this Chapter, the main findings and achievements of the present computational study, made with respect to the objective set in Chapter-1, are presented and the scope of extension and development of the present study are suggested. In Section 6.2, the summary of main findings and achievement are presented and the suggestions for future work are given in section 6.3. The flow parameters predicted for two entirely different types of rough texture, viz (i) saw tooth type, (ii) mean height type, following a smooth surface provides reasonably acceptable predictions.

6.2 Summary of Main Findings and Achievements

(a) The boundary layer thickness increases over the rough surface.

(b) The wall shear stress increases with the increase of surfaces roughness. The increase of wall shear stress for saw tooth type rough surface is much higher than the mean height type.

(c) The axial mean velocity profile is in good agreement for mean height type rough surface, while the shear stress in good agreement with the experimental dat for saw tooth type model of surface roughness.

(d) The static pressure shows a sharp jump at the rough smooth junction, followed by a steep decrease in the flow direction over the rough surface.

(e) The full details of the boundary layer development in transition from smooth to rough surface can not be reproduced by employing log-law or two-dimensional simulated rough texture.

6.3 Suggestions for Future Work

(i) The same prediction can be carried out with large number of fine grids which may reproduce more accurate result in details obtained by the experiment.

(ii) Higher order schemes (e.g. LUDS, Quick scheme) can be used to have better accuracy in this type of prediction.

(iii) To take account of the three-dimensional effect in the rough portion of the flow domain, three-dimensional calculation simulating the exact rough texture can be carried out.

(v) To obtain better results, turbulence models capable of handling this type of complicated flow can be used (e.g. Reynolds stress models, Large eddy simulation).

(vi) Similar study can be made with different types of roughness configurations.

(vii) Investigation can be made with modified (e.g. two-layer model: employ one-equation model in the near-wall region and the standard k-ε model in the core region of the flow) wall treatment.

REFERENCES

1. Ali, M.A.T. and Islam, O., "Development of a Turbulent Flow in a Smooth Pipe Following a Rough Pipe", Institution of Engineers Bangladesh, Vol. 10, No. 2, pp. 19, 1982.

2. Ali, M.A.T. and Islam, O., Flow in a Pipe Following an Abrupt Decrease in Surface Roughness" Proc. 12th South-eastern Conference on Theoretical and Applied Mechanics, Auburn University, 1984.

3. Ali, M.A.T. "Flow Through Square Ducts with Rough Ribs", Ph.D. Thesis, Imperial College, London, 1980.

4. Anderson, D.A.,Tannehill,J.C. and Pletcher,R.H., "Computational Fluid Mechanics and Heat Transfer. McGraw-Hill Book Co., New York, 1984.

5. Antonia, R.A. and Luxton, R.E., "The Response of a Turbulent Boundary Layer to a Step Change in Surface Roughness". Part 2. "Rough to Smooth", 2. Fluid Mechanics. Vol. 53, Part 4, pp. 737, 1972.

6. Antonia, R.A. and Luxton, R.E., "The Response of a Turbulent Boundary Layer to an Upstanding Step Change in Surface Roughness", Transactions of the ASME, 2. Basic Engineering, pp. 22, March 1971.

7. Antonia, R.A. and Wood, D.H., "Calculation of a Turbulent Boundary Layer Downstream of a Small Step Change in Surface Roughness", Aeronautical Quarterly, Vol. 28, pp. 202, 1975.

8. Antonia, R.A. and Luxton, R.E., "The Response of a Turbulent Boundary Layer to a Step Change in Surface Roughness. Part 1. Smooth to Rough", 2. Fluid Mechanics, Vol. 48, Part 4, pp. 721, 1971.

9. Brebbia, C.A. and Ferrante, A.J., "Computational Hydraulics", Butterworths, London, 1983.

10. Briley, W.R. " Numerical Method for Predicting Three-dimensional Steady Viscous Flow in Ducts", J.Comp. phys. Vol.14, pp.8-28, 1974.

11. Brundrett, E. and Baines, W.D, "The Production and Diffusion of Vorticity in Duct Flow", Department of Mechanical Engineering, University of Toronto, pp. 375. 1963.

12. Carl, E. Pearson, "A Computational Method for Viscous Flow Problems", J. Fluid Mech., Vol. 25, pp.611-622,1965.

13. Carper, H.J., "A Study of the Turbulent Intensities and Correlation Coefficients in the Incompressible Flow of Air in Transition From a Smooth

to Rough Wall in a Two-dimensional Channel", M.S. Thesis, The Agricultural and Mechanical College of Texas, 1972.

14. Chorin, A.J. "A Numerical Method for Solving Incompressible Viscous Flow Problems", J. Comp. phys. Vol.2, pp. 12-26, 1967.

15. Clauser, F.H., "The Turbulent Boundary Layer", Advances in Applied Mechanics, Vol. IV, Academic Press, 1956.

16. Clauser, F.H., " Turbulent Boundary Layer in Adverse pressure Gradient", 2. Aero Science, Vol. 21, pp. 91, 1954.

17. Deardorff, J.W. "A Numerical Study of Three-dimensional Turbulent Channel Flow at Large Reynolds Numbers", J. Fluid Mech., Vol. 41, pp.453-480, 1970.

18. Dodge, P.R. "Numerical Method for 2D and 3D Viscous Flows", AIAA J., Vol.15, pp.961-965, 1977.

19. Emery,A.F.and Gessner,F.B."The Numerical Prediction of the Turbulent Flow and Heat Transfer in the Entrance Region of a Parallel Plate Duct", J. Heat Transfer, Vol. 98, pp. 594-600,1976.

20. Floryan, J.M. and Dallmann, U. "Flow Over Leading Edge with Distributed Roughness". J.Fluid Mech., 1990, Vol. 216, pp. 629-656.

21. Fujita, H., "Turbulent Flows in Square Ducts Consisting of Smooth and Rough Planes", Research Reports of Faculty of Engg., Mie University, Vol. 3, 1978.

22. Furuya, Y. and Fufita, H., "Effect of Surface Roughness on Velocity Defect Law", The physics of Fluids Supplement, pp. 155, 1967.

23. Gosman, A.D. & Ideriah, F.J.K., "TEACH-T: A General Computer Program for Two-dimensional Turbulent, Recirculating Flows", Department of Mechanical Engineering, Imperial College, London, S.W.7, 1976.

24. Haldar, S.B., "Development of Turbulent Boundary Layer in Sudden Change of Upstanding Surface Roughness", M.Sc. Thesis,Bangladesh, University of Engineering and Technology,1987.

25. Hasan, A., "Study of Turbulent Boundary Layer in a Step Change From Smooth to Rough Surface". M.Sc. Thesis, Bangladesh University of Engineering & Technology, 1984.

26. Hinze, J.O., "Turbulence", 2nd edition, McGraw-Hill,New York, 1975.

27. Hinze, J.O., "Secondary Current in Wall Turbulence", The physics of fluids supplement, pp. 122, 1967.

28. Islam, O., "The Determination of the Turbulent Intensities in a Transitional Flow From a Smooth to a Rough Wall with Zero Pressure Gradient in a Two-dimensional Channel". M.S. Thesis, The Agricultural and Mechanical College of Texas, 1963.

29. Islam, O., and Logan, E., "Channel Flow Over a Smooth-to-Rough Surface Discontinuity with Zero Pressure Gradient", Transactions of the ASME, 2. Fluids Engg., pp. 626, Dec. 1976.

30. Jacobs, V.W., "Unformung Eines Turbulenten Geschwin-digkeitsprofiles", Z. Angew. Math. Mech., Vol. 19, pp. 87, 1939.

31. Khalil, G.M. "The Initial Region of a Plane Turbulent-mixing Layer", Ph.D. Thesis, Bangladesh University of Engineering and Technology, 1983.

32. Klebanoff, P.S., "Characteristics of Turbulence in a Boundary Layer with Zero Pressure Gradient", NACA Technical Report No. 3187, 1954.

33. Klinksiek, W.F. and Pierce, F.J. "A Finite-Difference Solution of the Two and Three- dimensional Incompressible Turbulent Boundary Layer Equations", J. Fluids Eng., Vol. 95, pp. 445-458, 1973.

34. Laufer, J., "Investigation of Turbulent Flow in a Two-Dimensional Channel", NACA Report No. 1053, 1951.

35. Launder, B.E. and Spalding, D.B. "Mathematical Models of Turbulence ", Academic, New York, 1972.

36. Launder, B.E. and Spalding, D.B. "The Numerical Computation of Turbulent Flows ", Comput. Methods Appl. Mech. Eng., Vol. 3, pp. 269-289, 1974.

37. Logan, E., and Jones, J.B., "Flow in a Pipe Following an Abrupt Increase in Surface Roughness", Transactions of the ASME, 2. Basic Engineering, pp. 1, March 1963.

38. Naser, J.A., "Development of Turbulent Boundary Layer in Sudden Step Change of Surface Roughness", M.Sc. Thesis, Bangladesh, University of Engineering and Technology, 1985.

39. Nikuradse, J., "Laws for Flow in Rough Pipes", NACA Technical Memorandum, pp. 1292, 1950.

40. Patankar, S.V. "Numerical Heat Transfer and Fluid Flow", Hemisphere, Washington, D.C., 1980.

41. Patankar, S.V. and Spalding, D.B. "Heat and Mass Transfer in Boundary" Layers, 2nd. edition, Intertext Books, London, 1970.

42. Perry, A.E., and Joubert, P.N., "Rough-wall Boundary Layers in Adverse Pressure Gradients", 2. Fluid Mechanics, Vol. 17, Part. 2, pp. 193, 1963.

43. Perry, A.E., Schofield, W.H. and Joubert, P.N., "Rough Wall Turbulent Boundary Layers", 2. Fluid mechanics, Vol. 37, Part 2, pp. 383, 1969.

44. Pletcher, R.H. "Prediction of Turbulent Boundary Layers at Low Reynolds Numbers", AIAA J., Vol. 14, pp. 696-698, 1976.

45. Pletcher, R.H. "Prediction of Incompressible Turbulent Separating Flow", J. Fluids Engg., Vol. 100, pp. 427-433, 1978.

46. Potter David, "Computational Physics", A Wiley-Interscience Publication, London, 1973.

47. Reichard, H., "Messungen Turbulenten Schwankungen", Naturwissenschaften, pp. 404, 1938.

48. Roache, P.J. "Computational Fluid Dynamics", Hermosa, Albuquerque, New Mexico, 1972.

49. Robertson, J.M., "The Turbulent Velocity Distribution in Rough Pipe", 5th Mid Western Conference on Fluid Mechanics, pp. 67, 1957.

50. Schlichting, H., "Boundary-Layer Theory", 7th edition, MacGraw-Hill, New York, 1979.

51. Schofield, W.H., "Measurements in Adverse-Pressure-Gradient Turbulent Boundary Layers with a Step Change in Surface Roughness", 2. Fluid Mechanics, Vol. 70, Part 3, pp. 573, 1975.

52. Siuru, W.D. and Logan, E., "Response of a Turbulent Pipe Flow to a Change in Roughness", Transactions of the ASME, 2. Fluids Engg., pp. 548, Sept. 1977.

53. Tannehill, J.C. and Anderson, D.A., "Computation of Three-dimensional Supersonic Viscous Flows in Internal Corners", Technical Report AFWAL-TR-80-3017, 1980.

54. Thomas, D.L., and Easter, P.G., "Measurement of Wall Shear Stress in a Duct of Square Cross-Section", CEGB Report, Berkeley Nuclear Laboratories, R&D Dept. RD/B/N 2477, 1972.

55. Townes, H.W., and Sebersky, R.H., "Experiments on the Flow Over Rough Surface", International 2, Heat and Mass Transfer, Vol. 9, pp. 729, 1966.

56. Tracy, H.J., "Turbulent Flow in a Three-dimensional Channel", Journal of the Hydraulics Division, Proceedings of the American Society of Civil Engineers, pp. 9, Nov. 1965.

57. Uddin, A.K.M., "Development of Turbulent Boundary Layer in Sudden Change of Depressed Surface Roughness". M.Sc. Thesis, Bangladesh, University of Engineering and Technology, 1986.

58. White, F.M. "Viscous Fluid Flow", MacGraw-Hill, New York, 1974.

59. Wirz, H.J. and Smolderen, J.J. "Numerical Methods in Fluid Dynamics", McGraw-Hill , New York, 1978.

60. Wood, D.H., and Antonia, R.A., "Measurements in Turbulent Boundary Layer Over a d-type Surface Roughness", Transactions of the ASME, 2. Applied Mechanics, pp. 591, Sept. 1975.

61. Yuan, S.W. "Foundation of Fluid Mechanics", McGraw-Hill, New York.

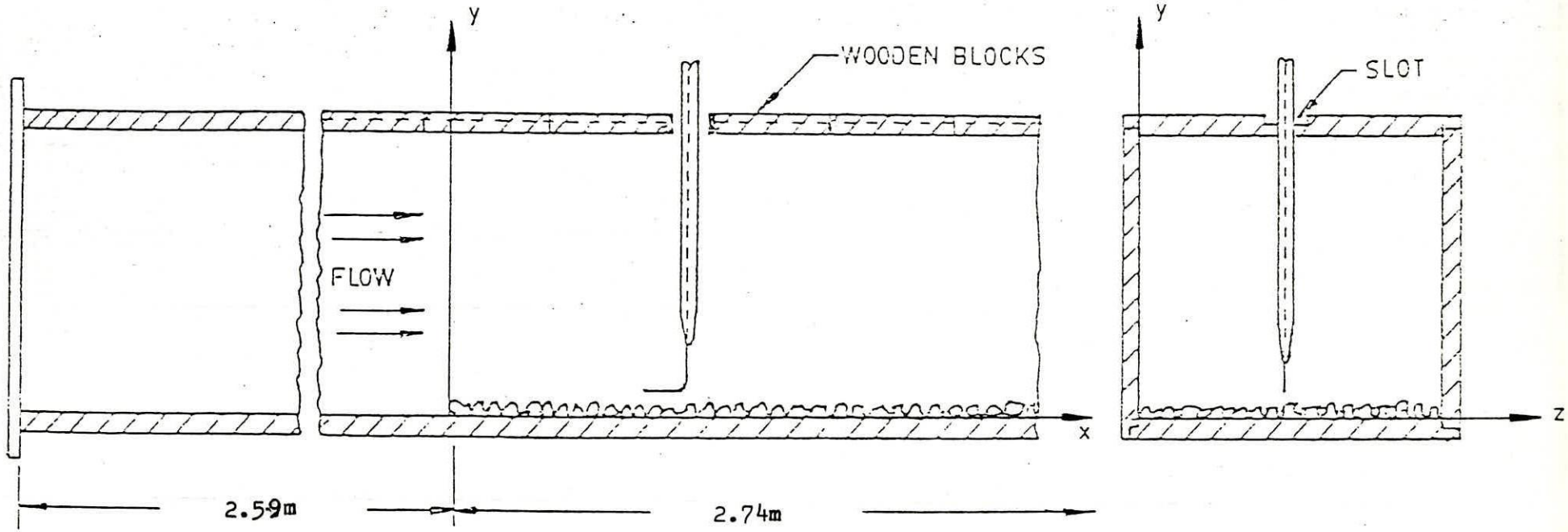

Fig. 1 Experimental Test Section of Naser (1985).

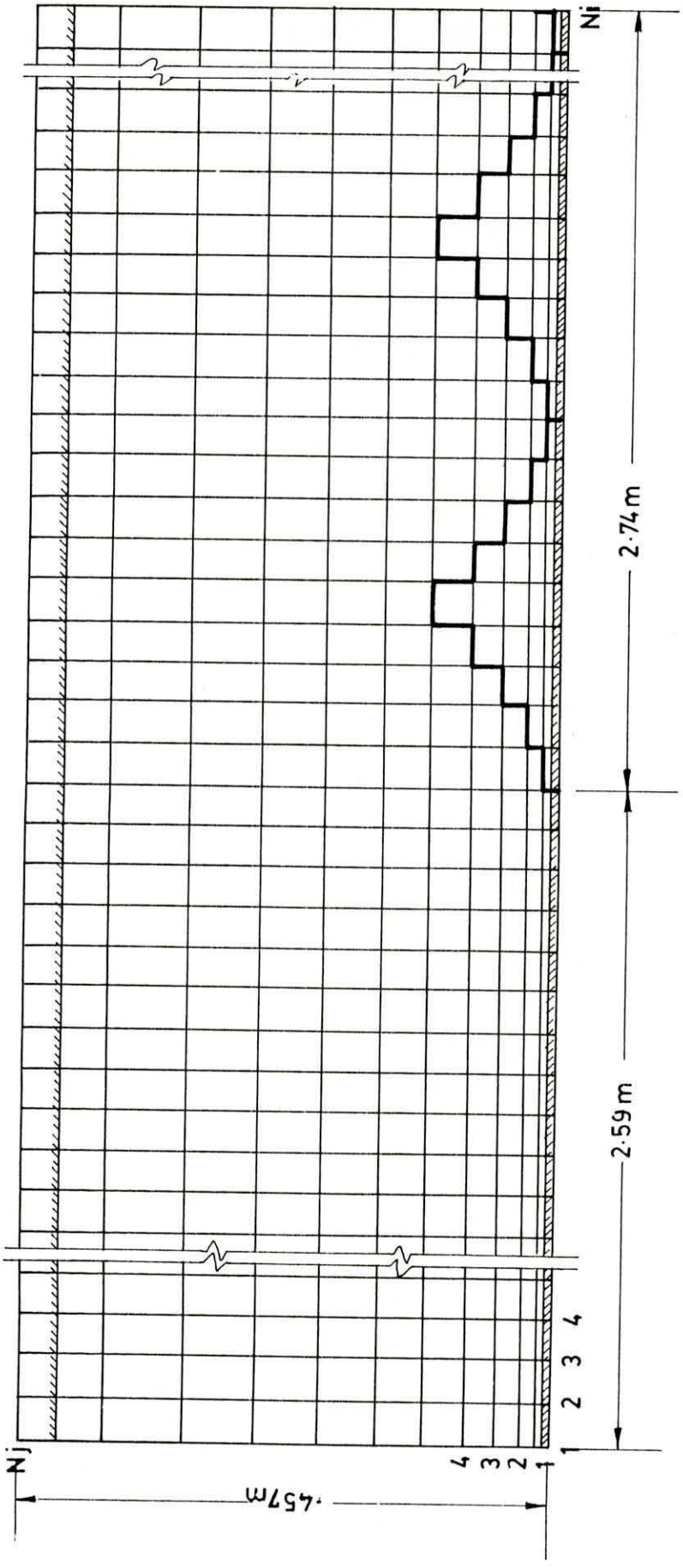

FIG 2(a) COMPUTATIONAL GRID (SAW TOOTH TYPE)

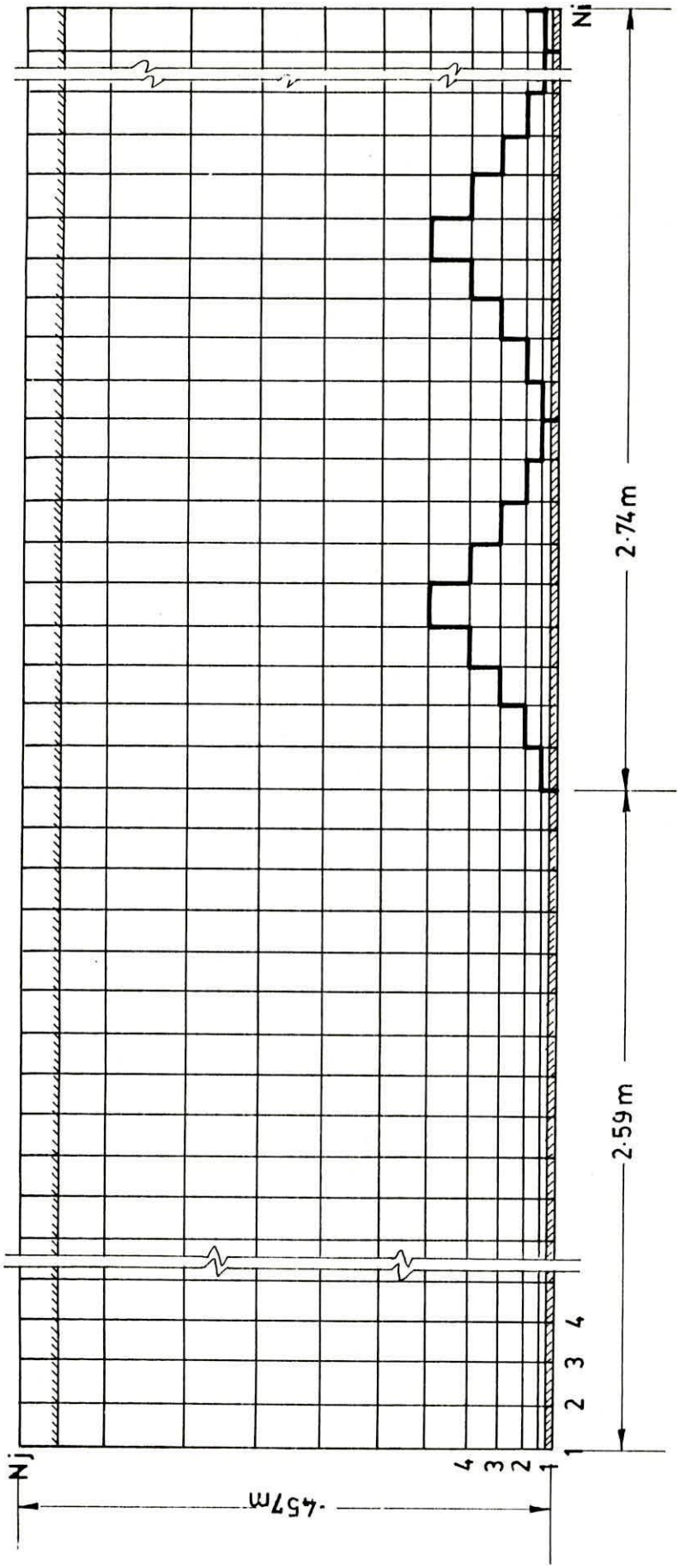

FIG 2(a) COMPUTATIONAL GRID (SAW TOOTH TYPE)

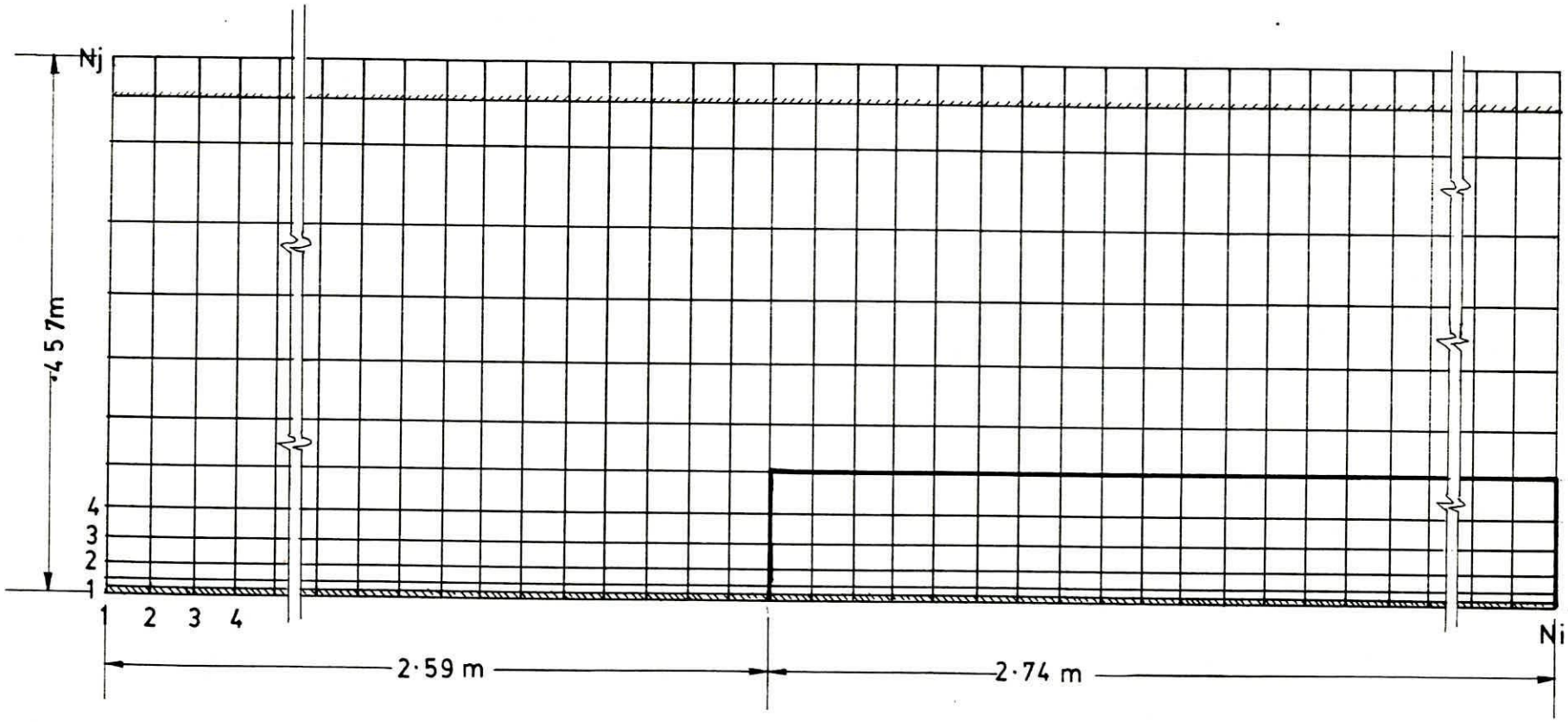

FIG. 2(b) COMPUTATIONAL GRID (MEAN HEIGHT TYPE)

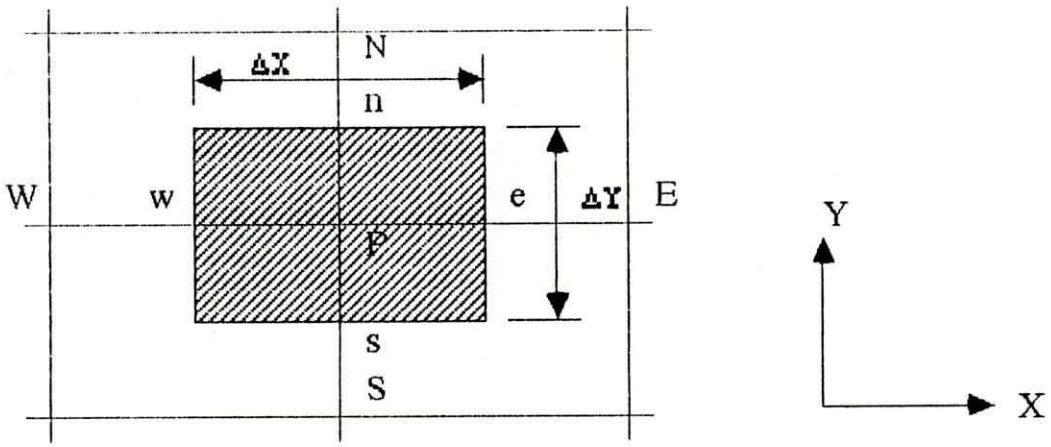

Fig. 3.1 : Two dimensional computational cell.

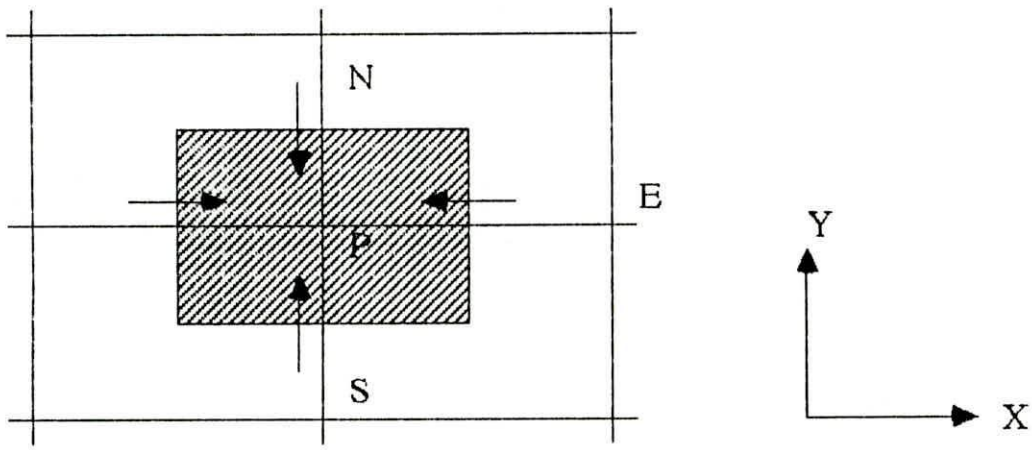

Fig. 3.2 : Control volume for continuity equation.

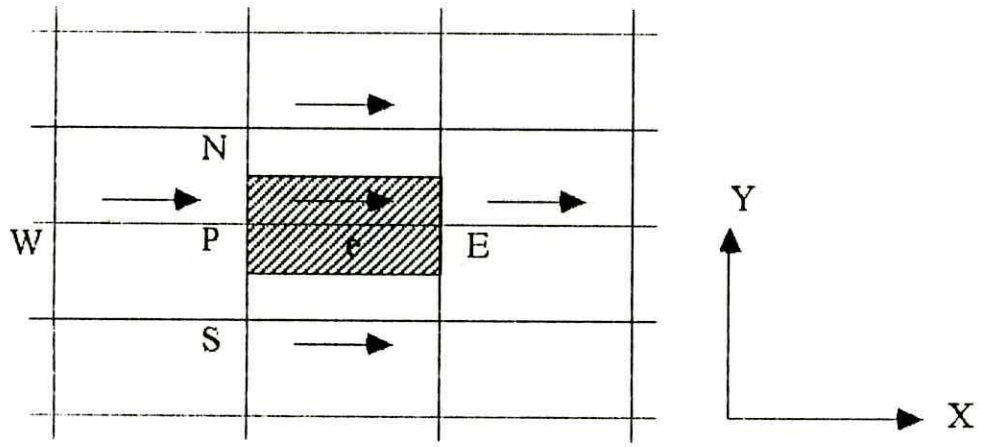

Fig. 3.3 : Control volume for U

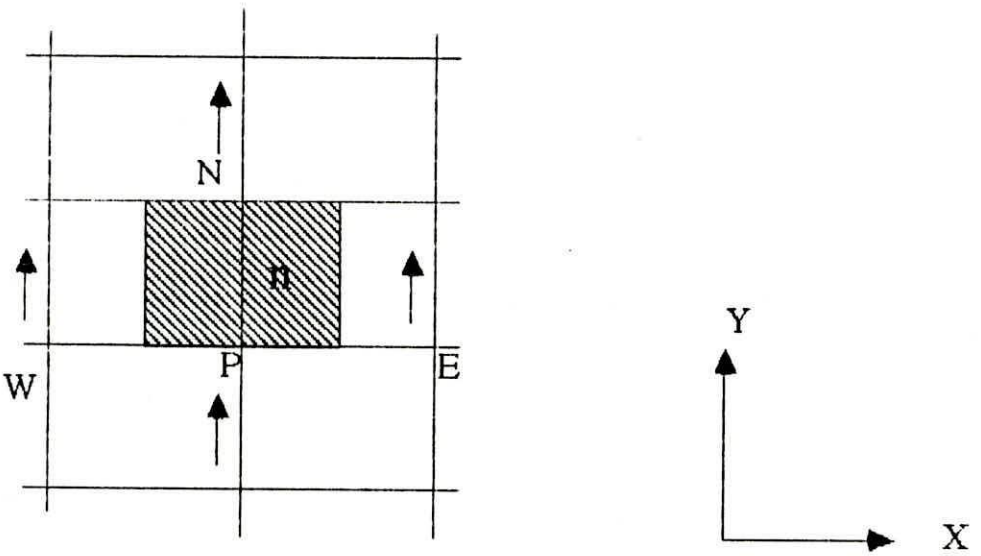

Fig. 3.4 : Control volume for V

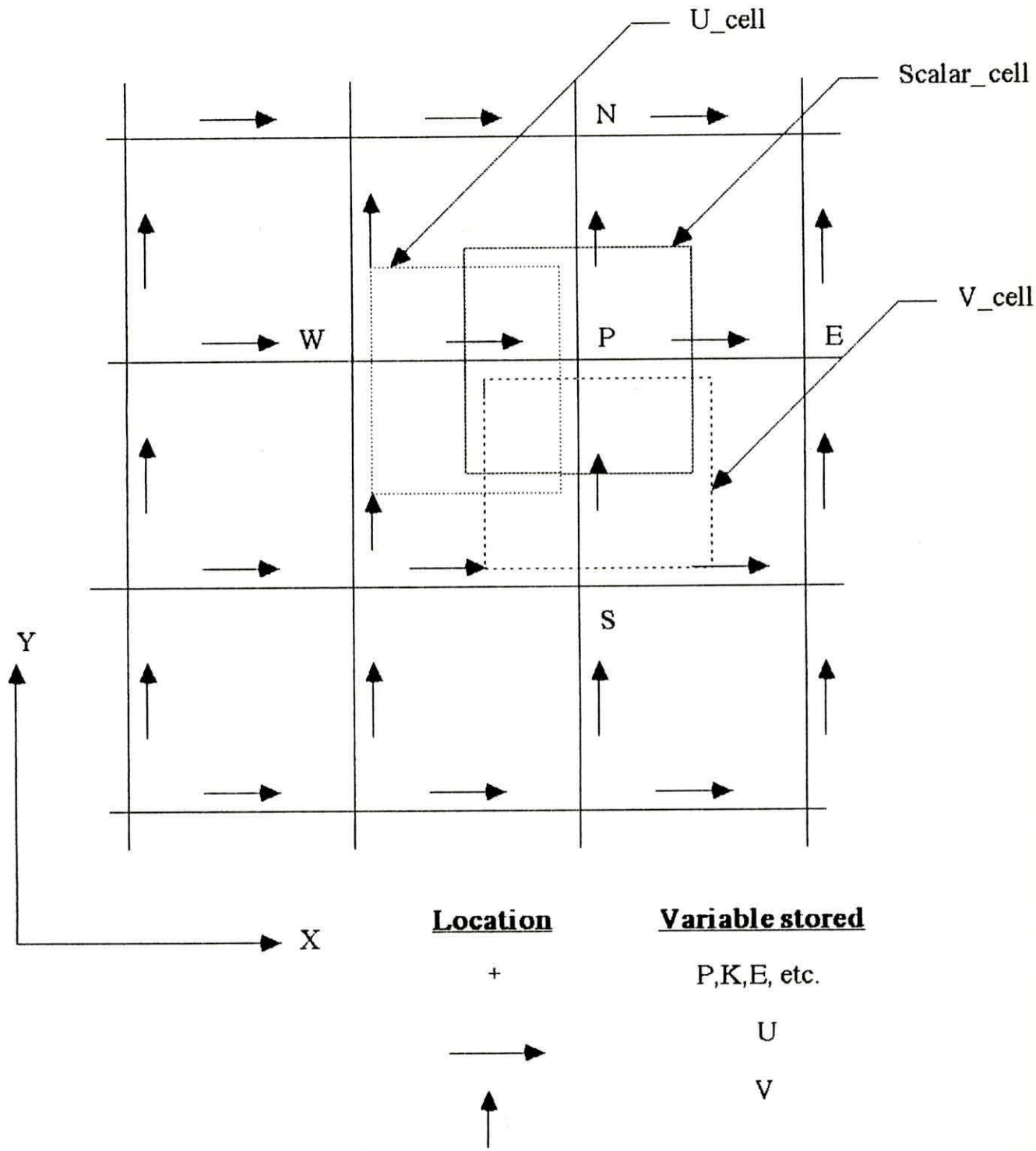

Fig. 3.5 : Computational grid, location and control volumes (cells) of scalar variables and axial and radial velocities.

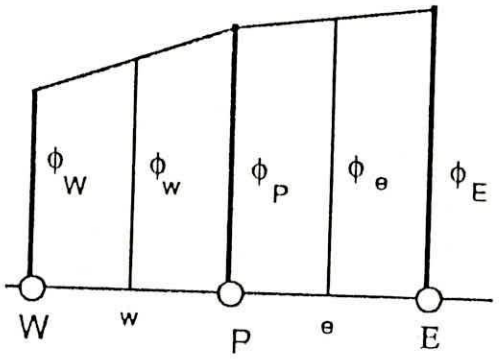

Fig. 3.6: Schematic presentation of CDS

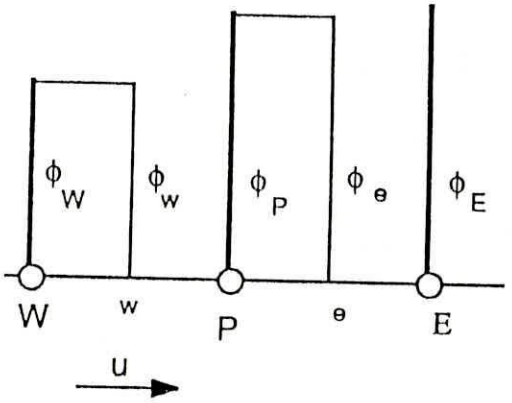

Fig. 3.7: Schematic presentation of UDS

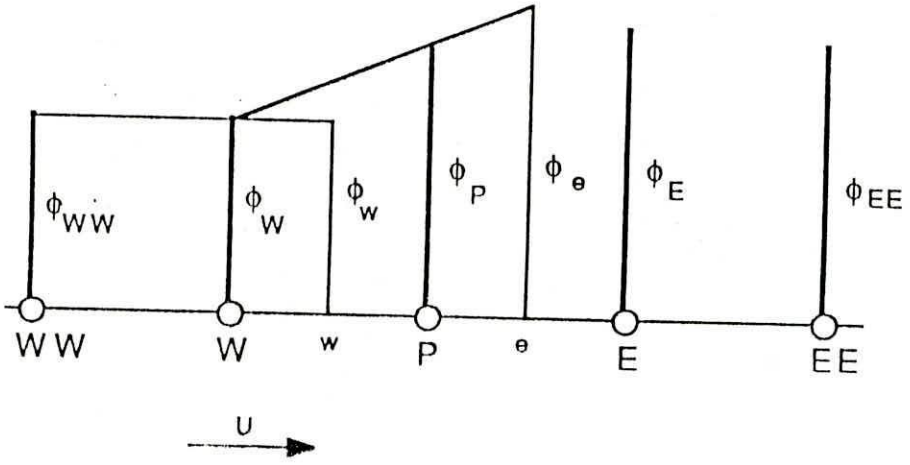

Fig. 3.8: Schematic presentation of LUDS

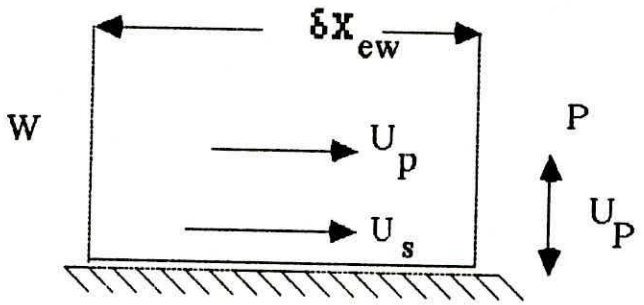

Fig. 3.9 Incorporation of wall boundary condition for Momentum equation

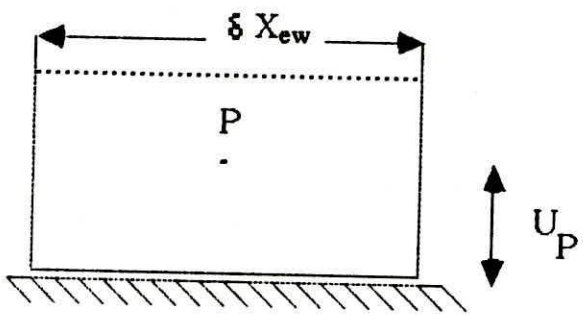

Fig. 3.10 Incorporation of wall boundary condition for turbulance energy

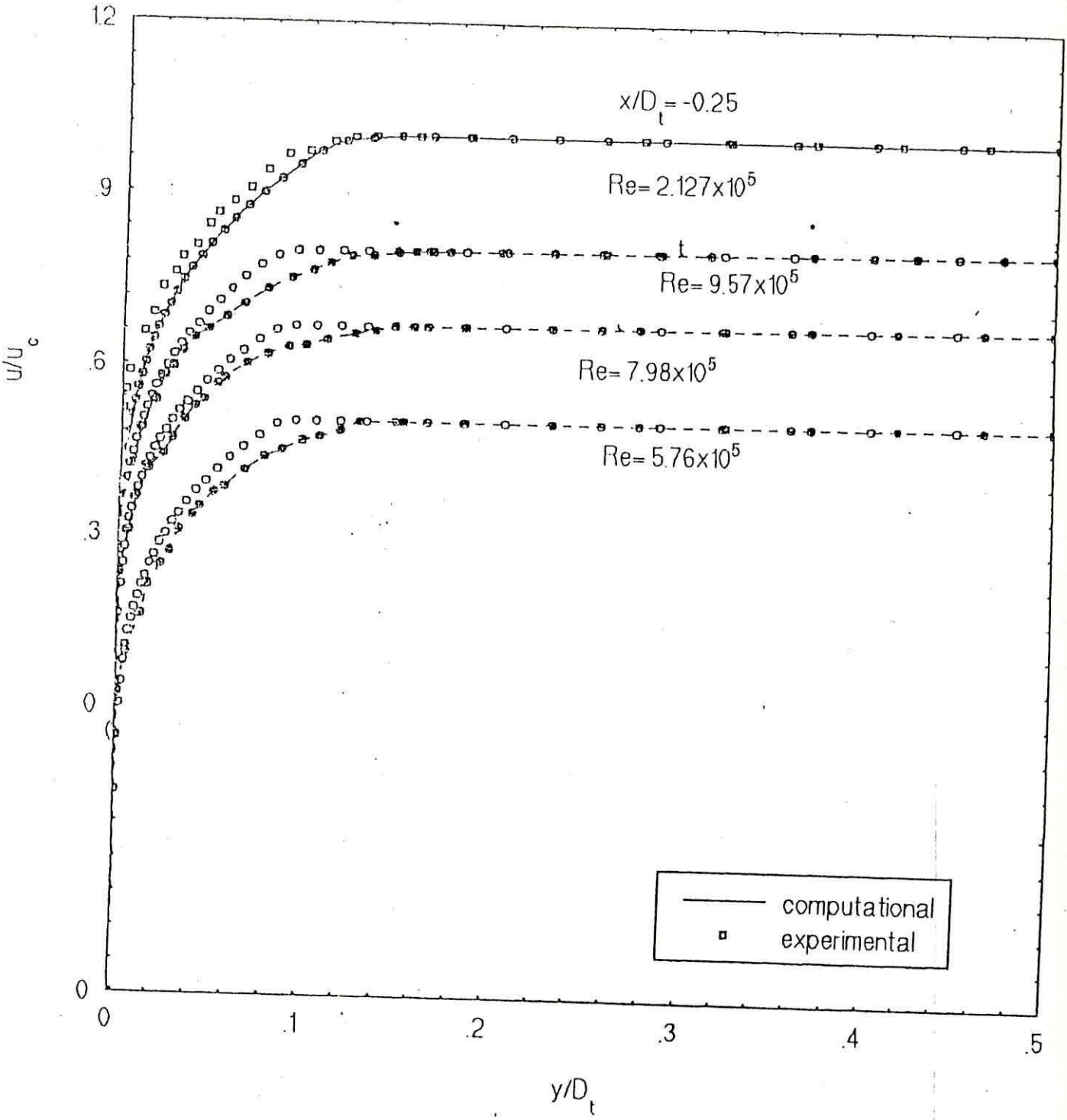

Fig. 4.1(a) Mean velocity profile over smooth surface at x/D_t = -0.25

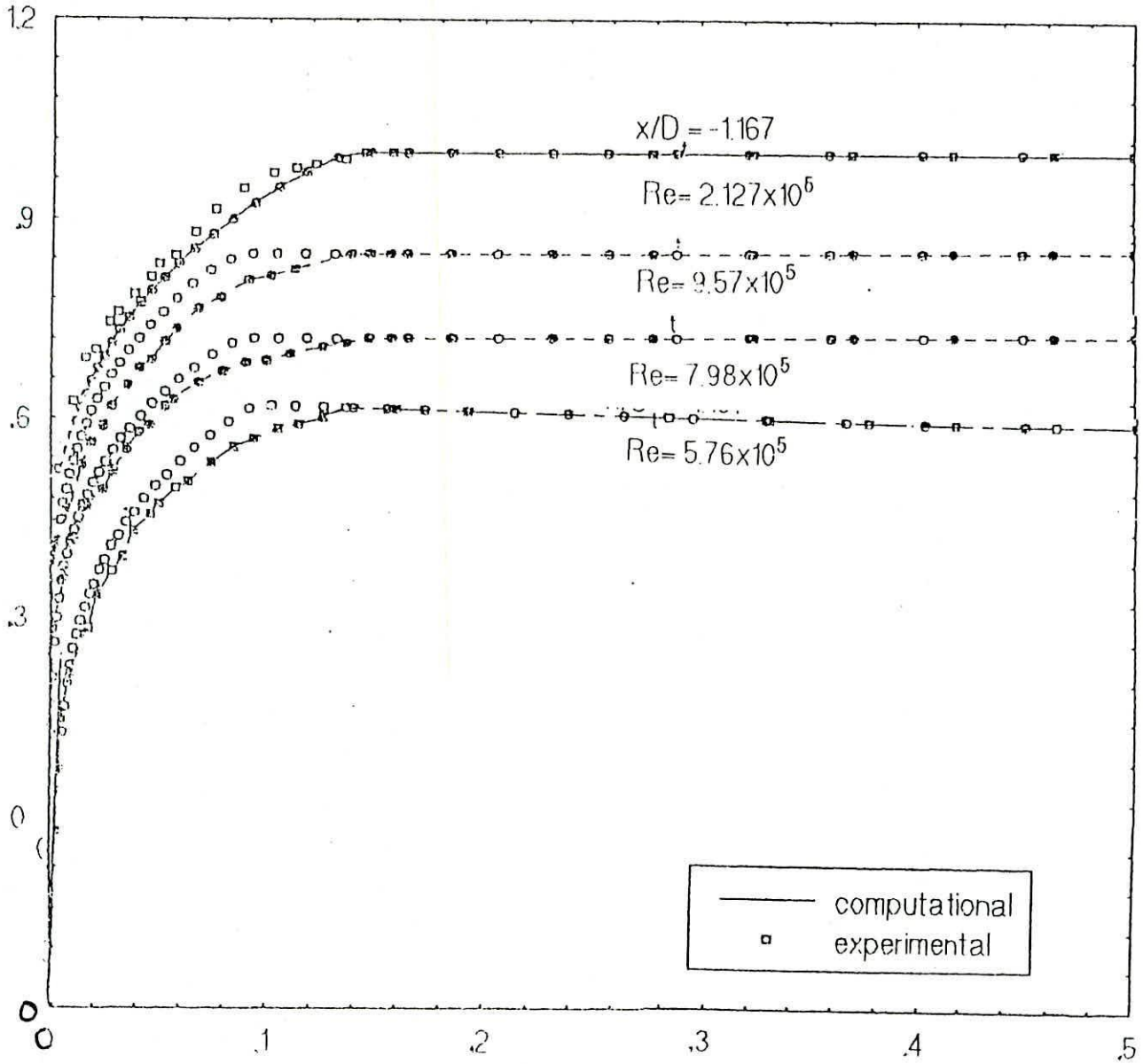

Fig. 4.1(b) Mean velocity profile over smooth surface at x/D_t = - 1.167

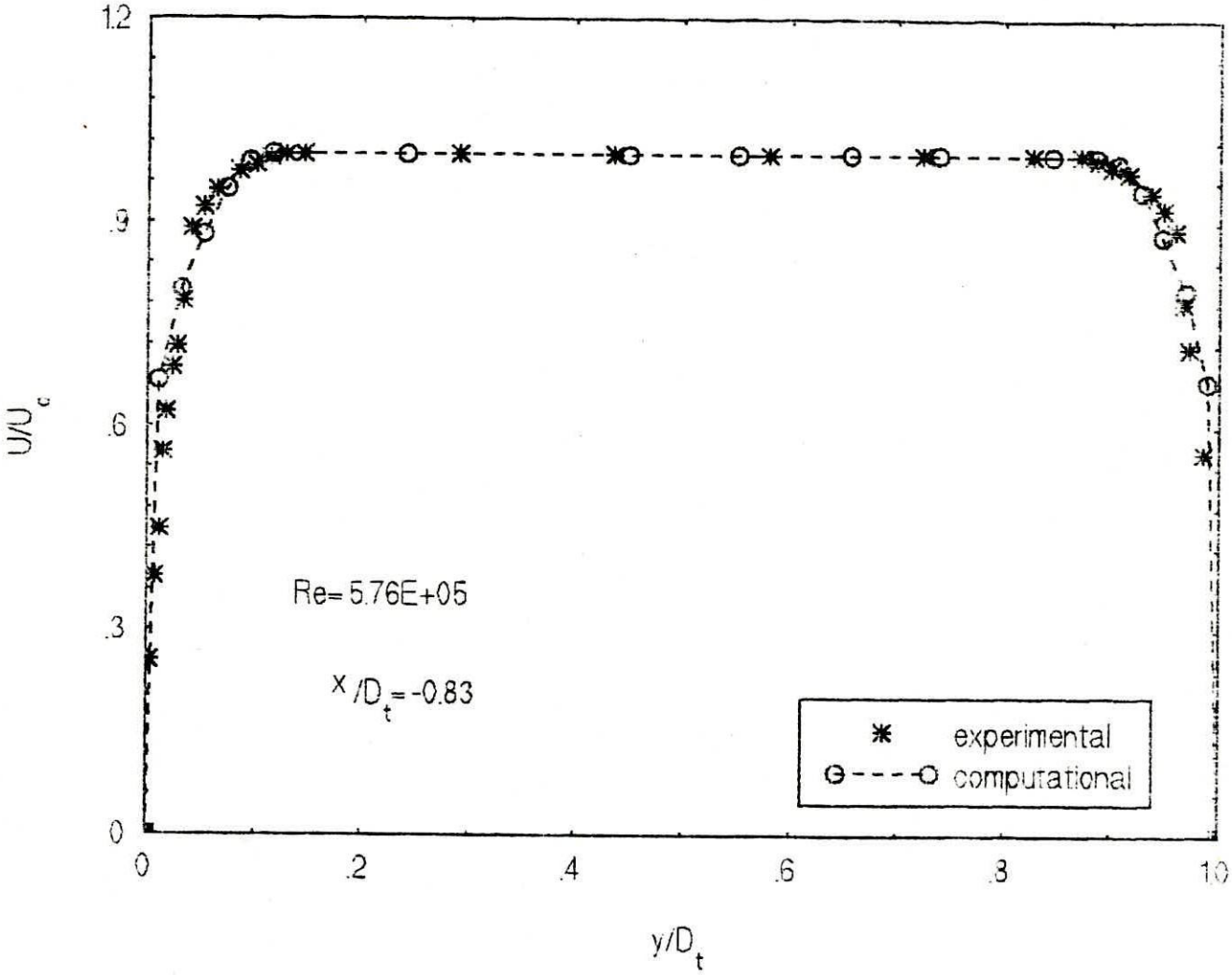

Fig. 4.2 Mean velocity profile (over the entire-diameter) over smooth surface at $x/D_t = -0.83$

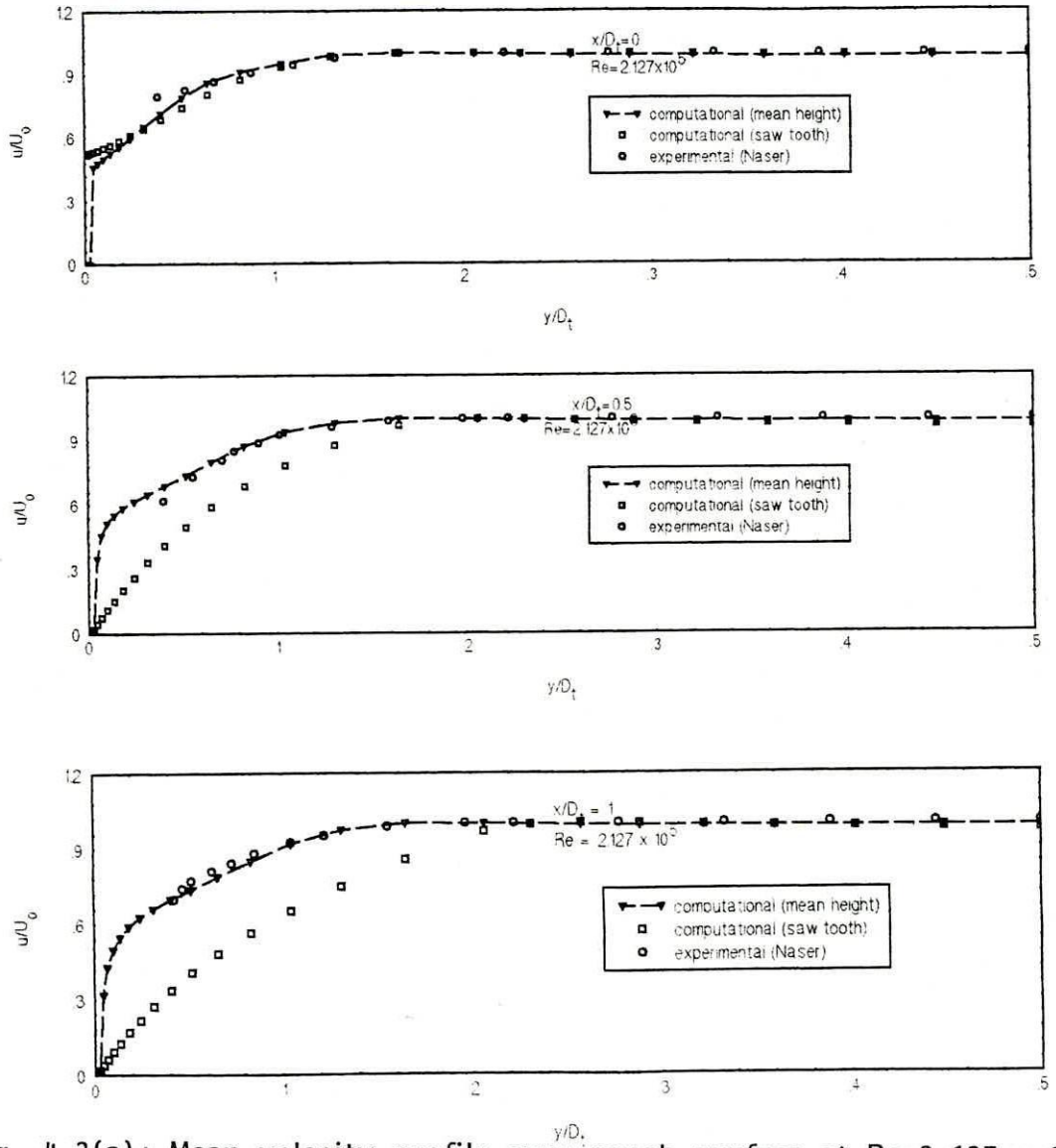

Fig. 4.3(a): Mean velocity profile over rough surface at Re=2.127 x 10^5

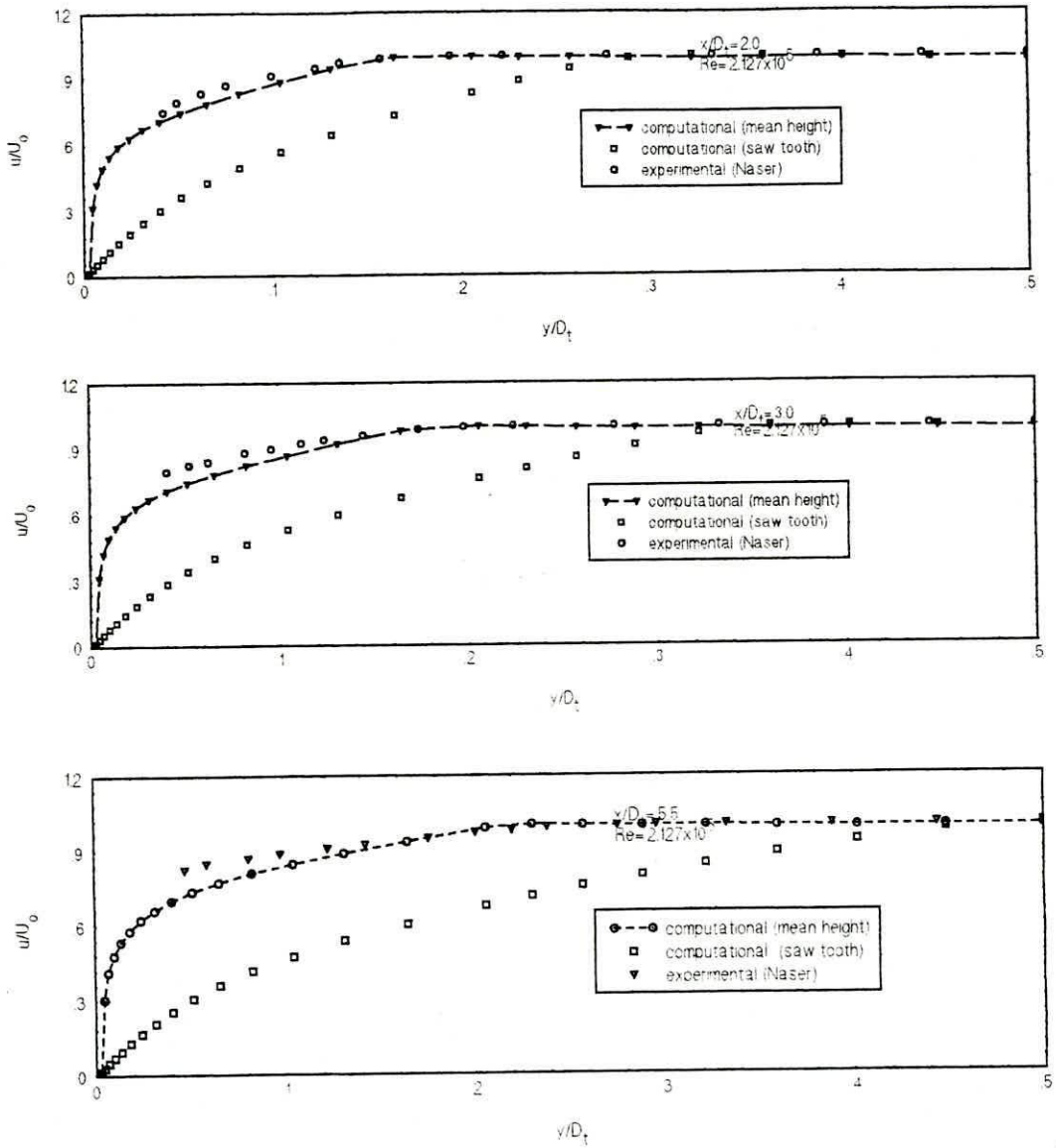

Fig. 4.3(b): Mean velocity profile over rough surface at Re=2.127 x 10^5

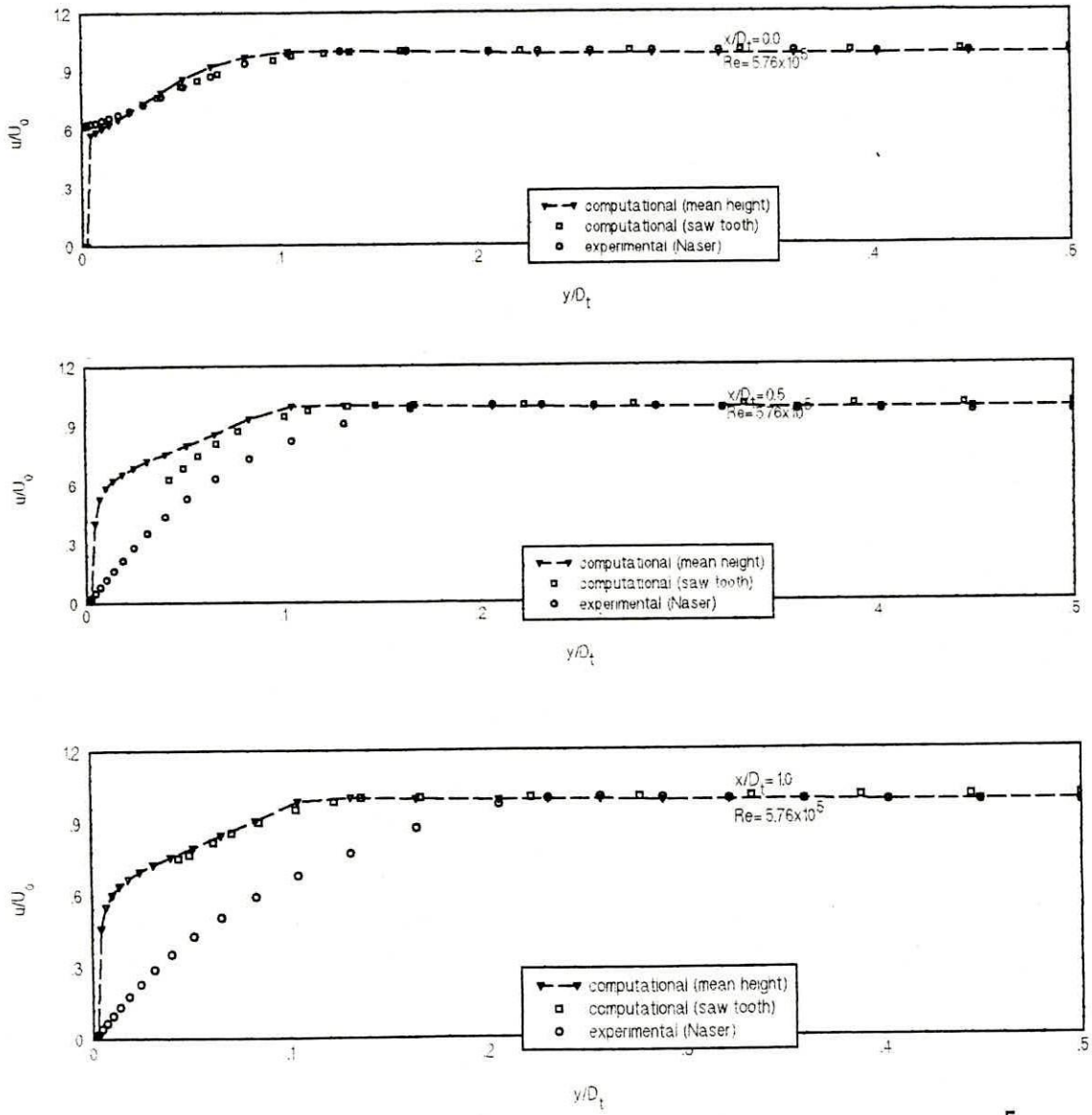

Fig. 4.3(c): Mean velocity profile over rough surface at Re = 5.76 x 10^5

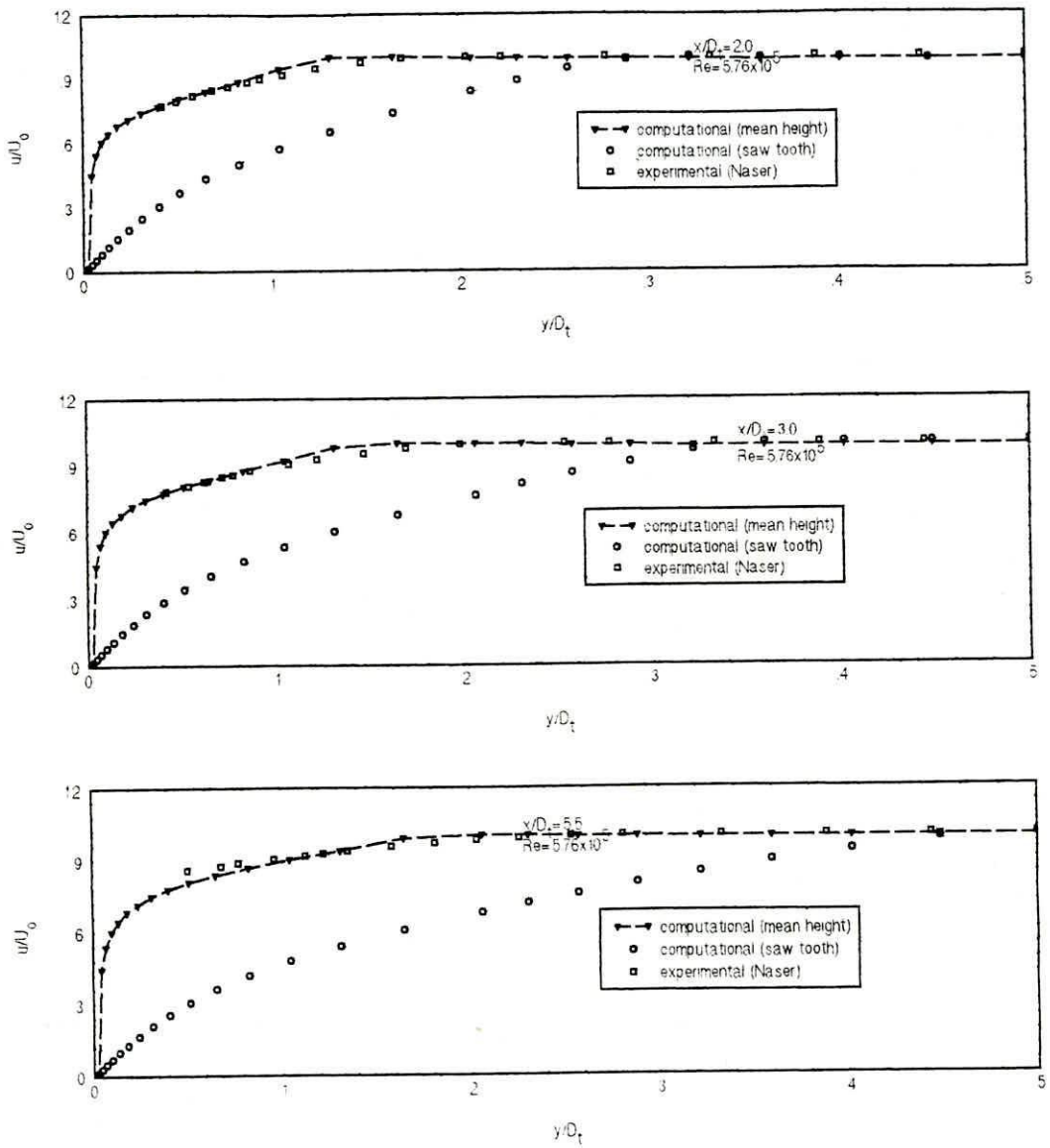

Fig. 4.3(d): Mean velocity profile over rough surface at Re = 5.76 x 10^5

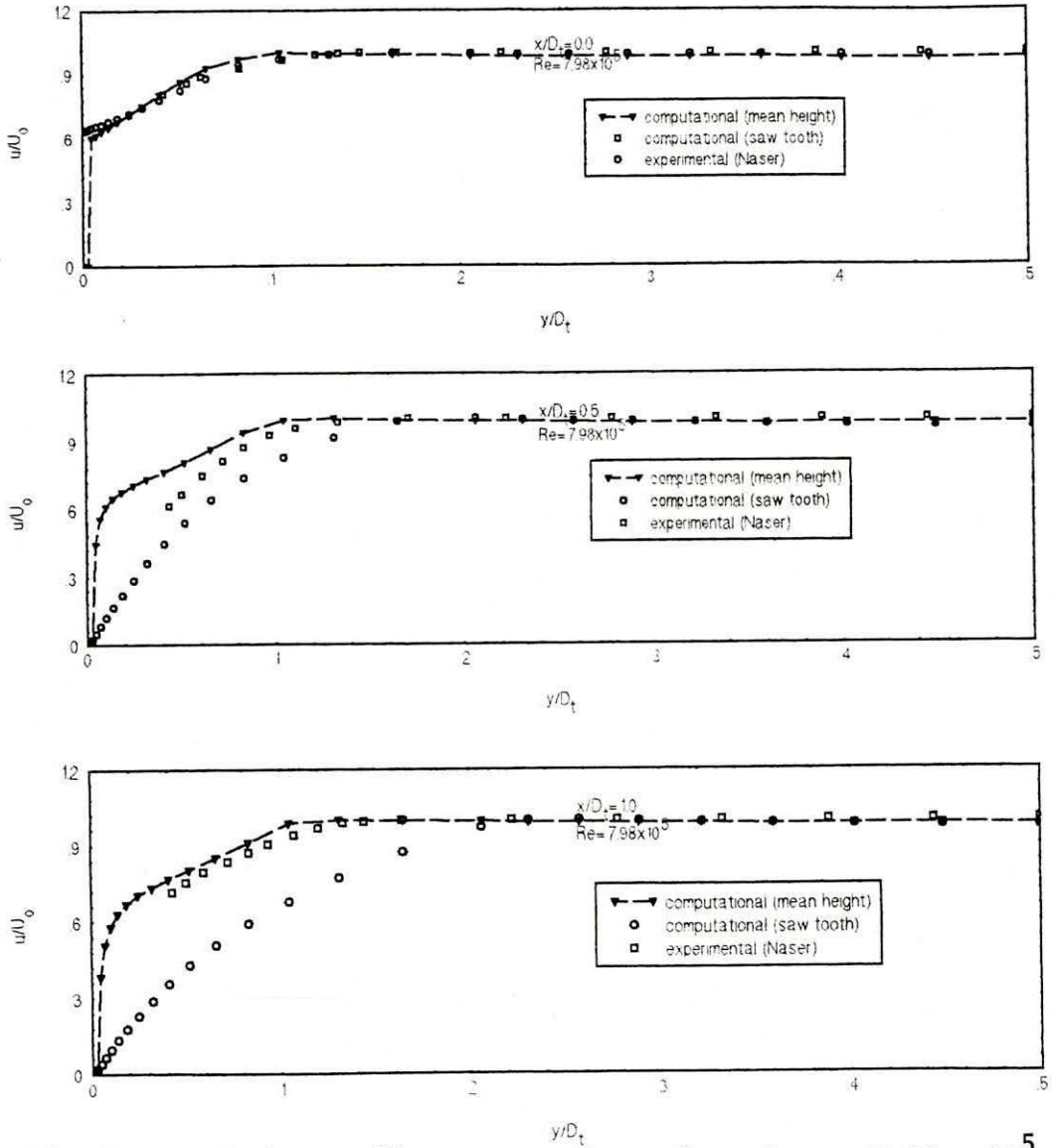

Fig. 4.3(e): Mean velocity profile over rough surface at $Re = 7.98 \times 10^5$

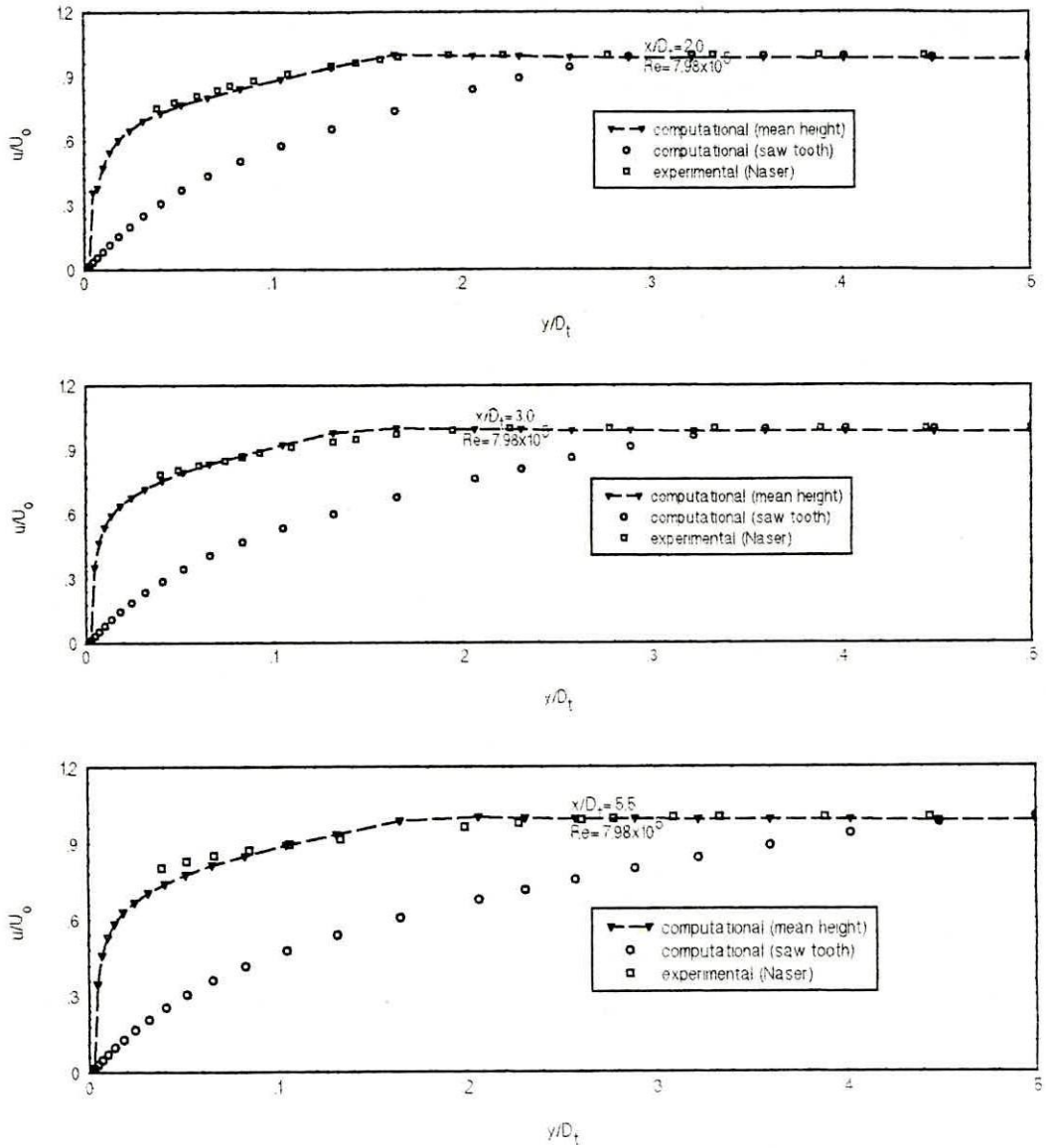

Fig. 4.3(f): Mean velocity over rough surface at Re = 7.98×10^5

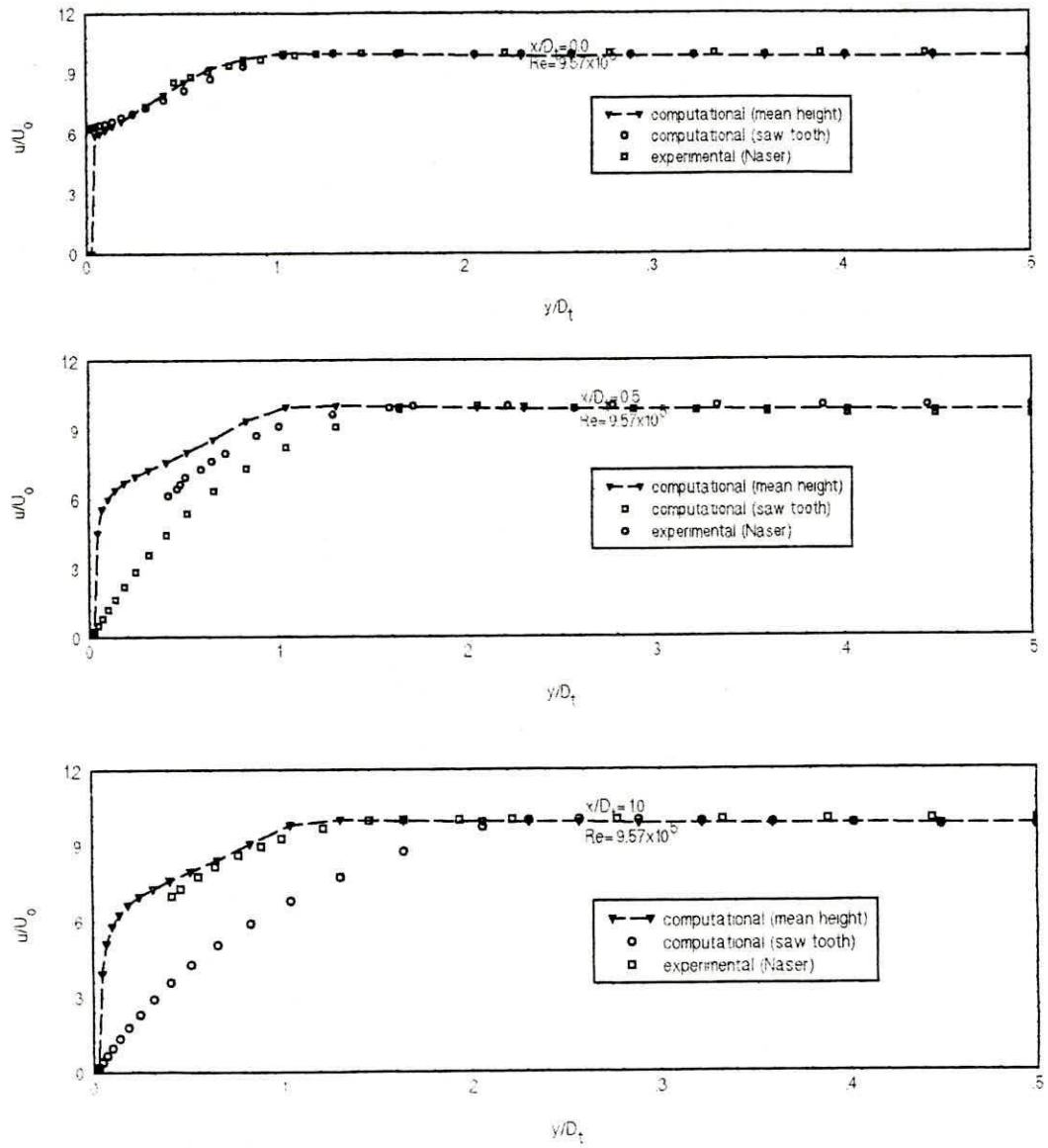

Fig. 4.3(g): Mean velocity profile over rough surface at Re = 9.57 x 10^5

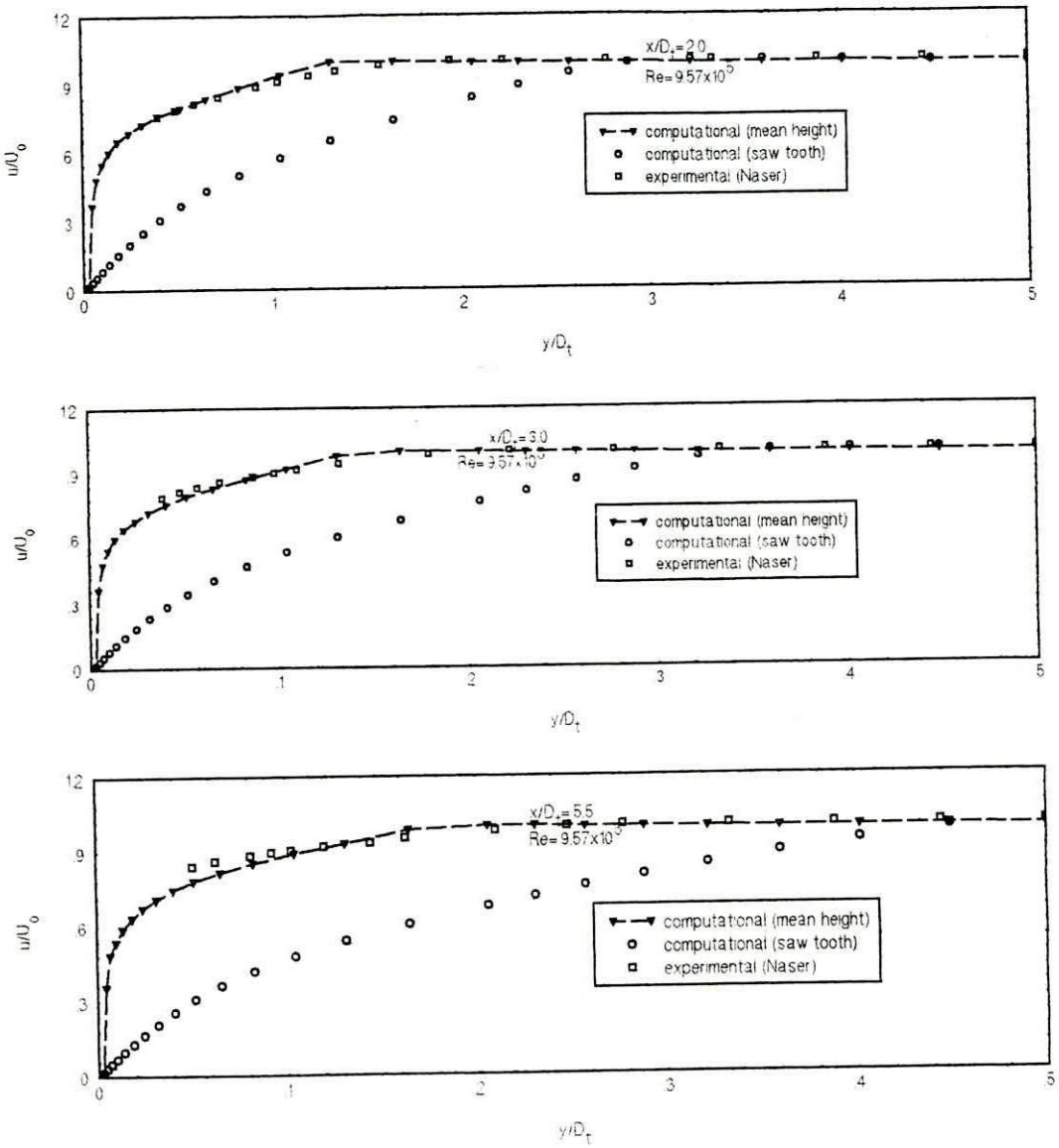

Fig. 4.3(h): Mean velocity profile over rough surface at Re = 9.57×10^5

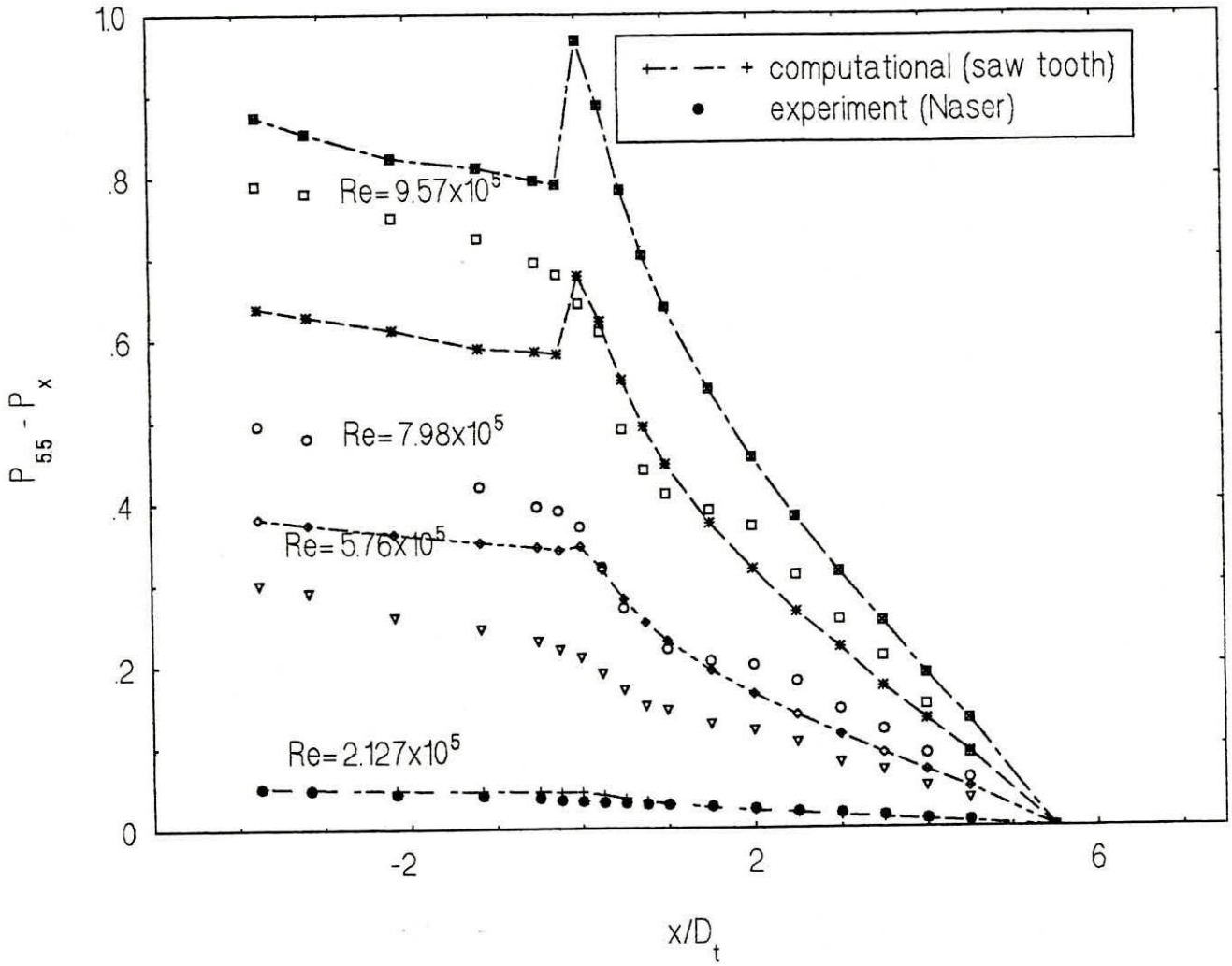

Fig. 4.4(a): Pressure gradient along the direction of flow (Saw tooth).

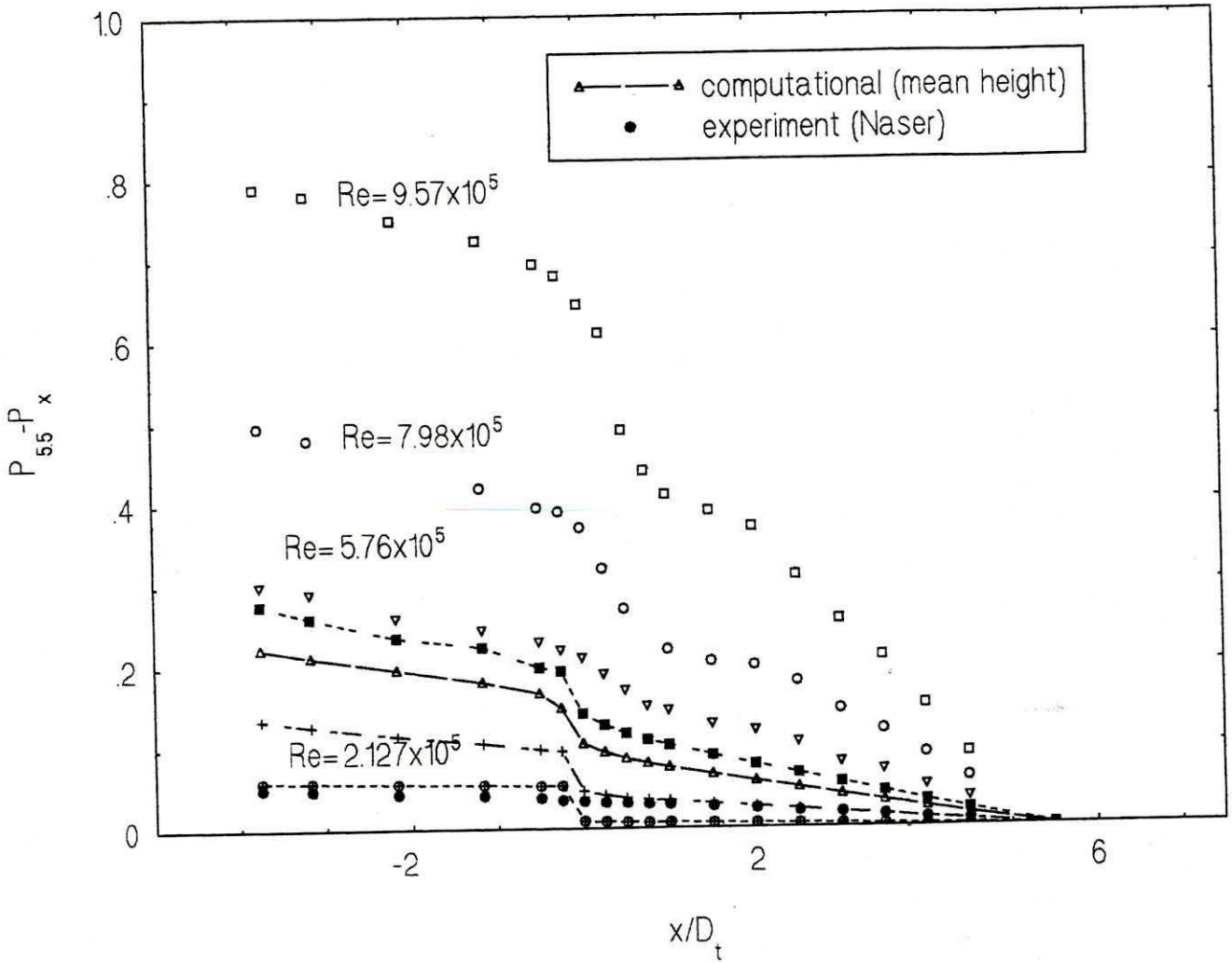

Fig. 4.4(b): Pressure gradient along the direction of flow (Mean height).

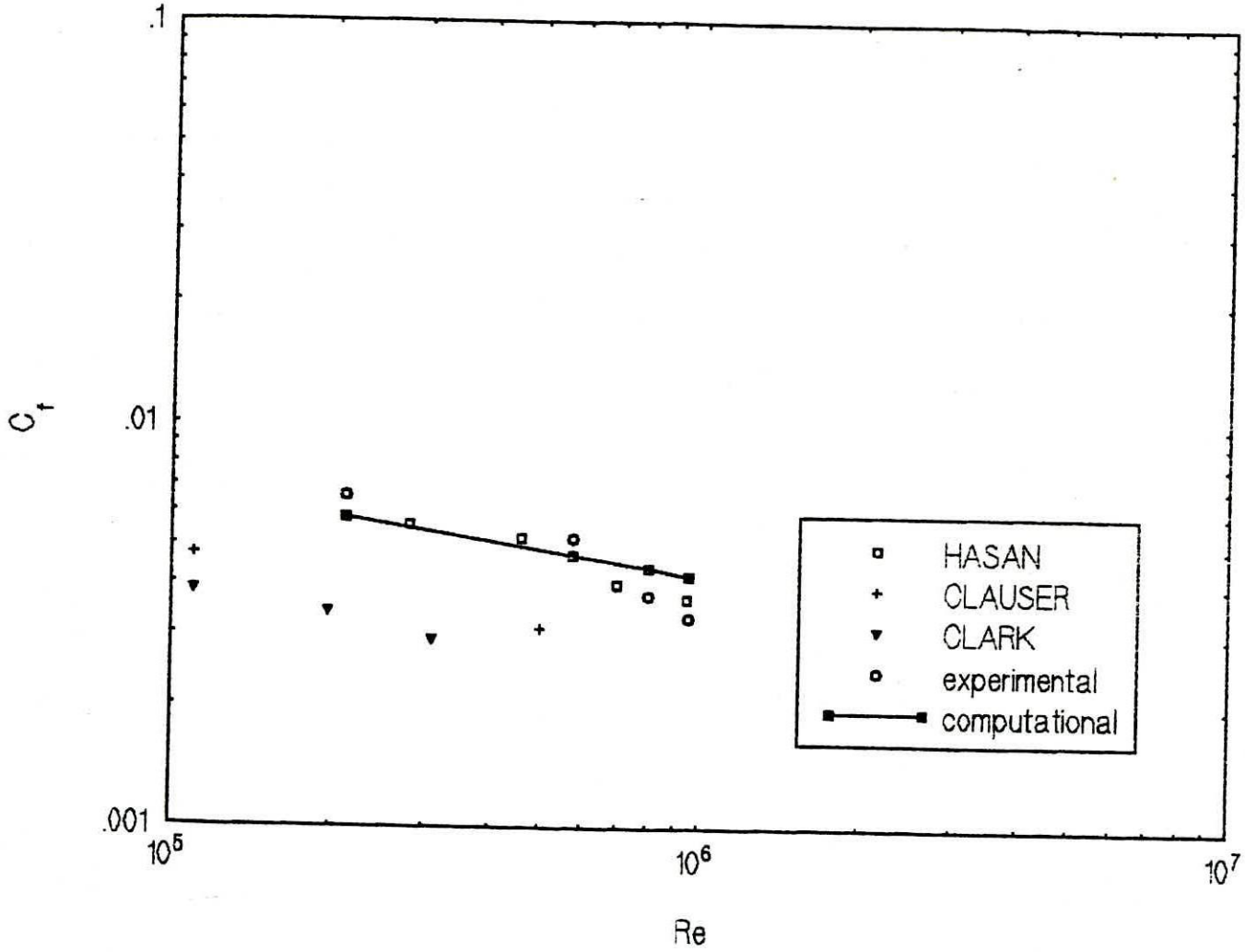

Fig. 4.5 Friction factor Vs Reynolds number for smooth surface

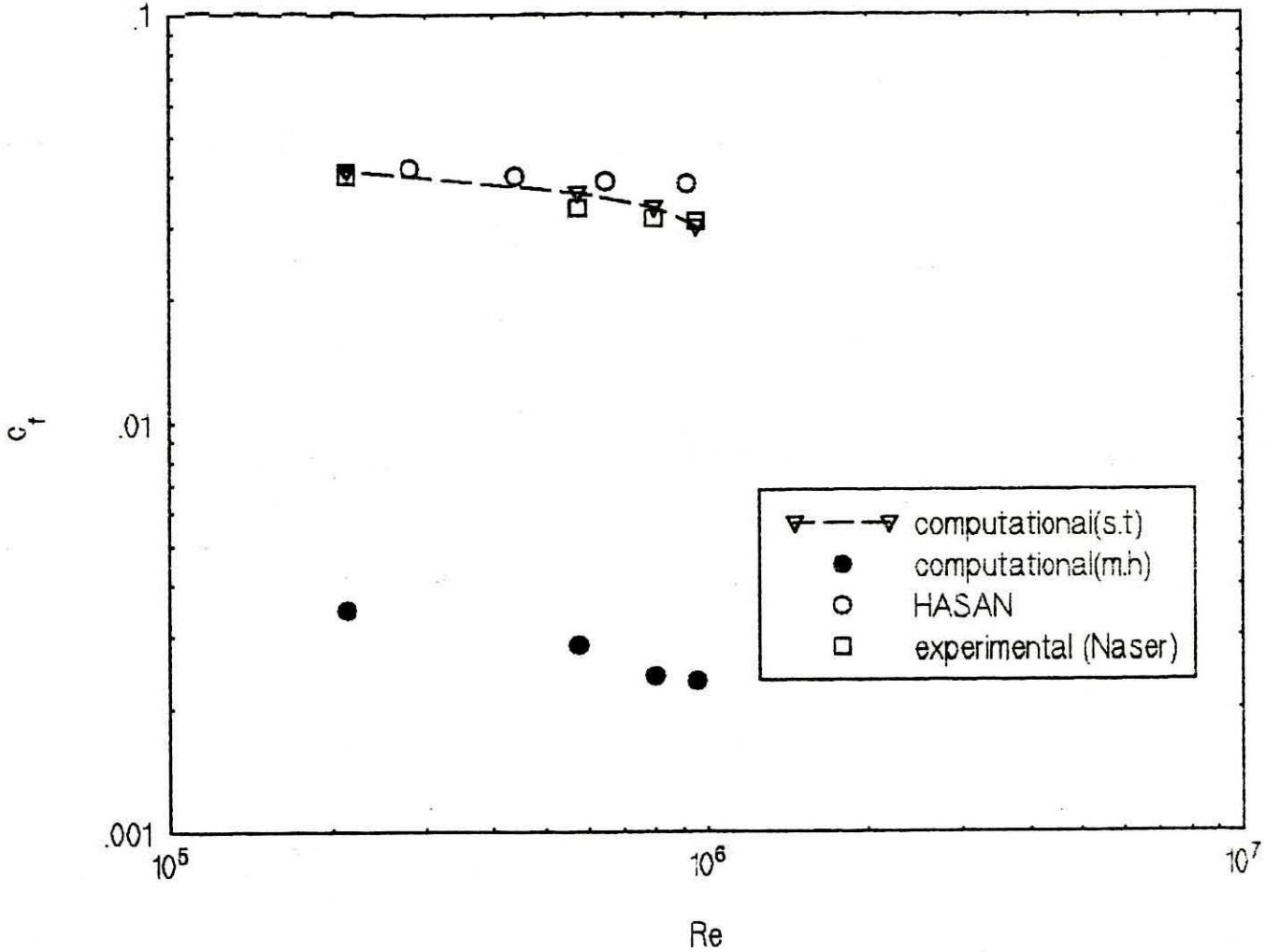

Fig. 4.6 Friction factor Vs. Reynolds number for Rough surface

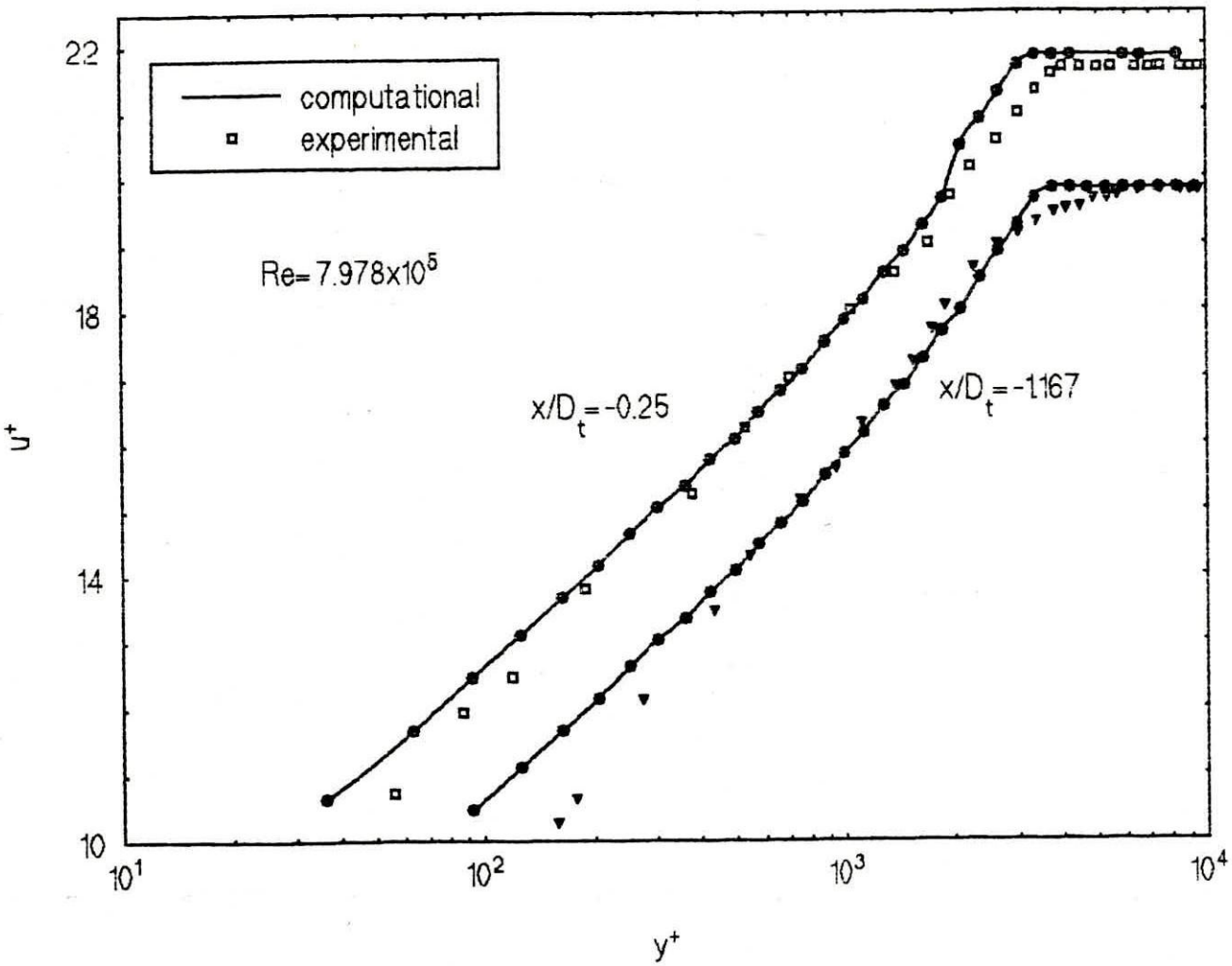

Fig. 4.7(a) Logarithmic velocity profile near the smooth surface at Re=7.978x10^5

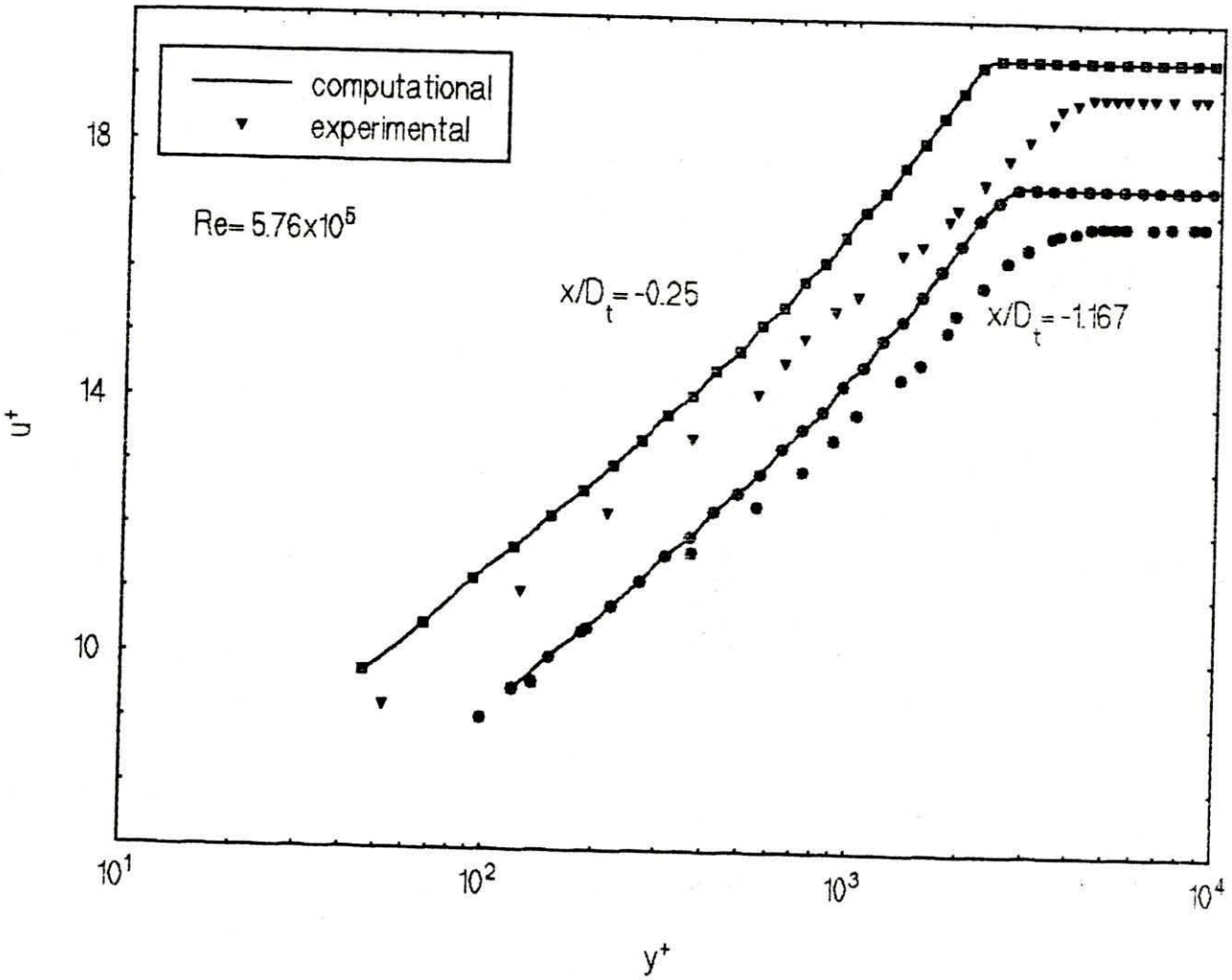

Fig. 4.7(b) Logarithmic velocity profile near the smooth surface at $Re=5.76X10^5$

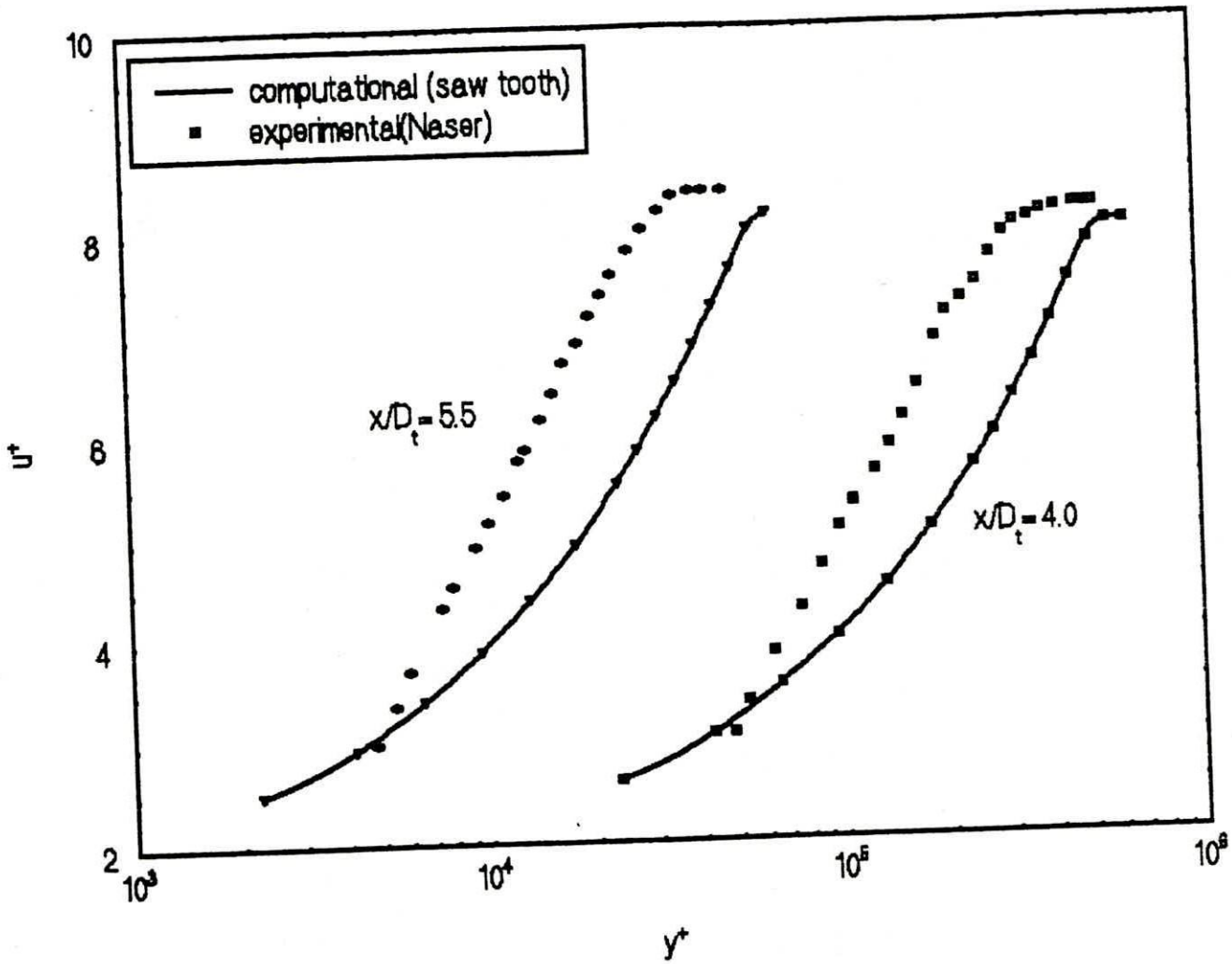

Fig. 4.8(a) Logarithmic velocity profile over the rough surface (Saw-tooth)

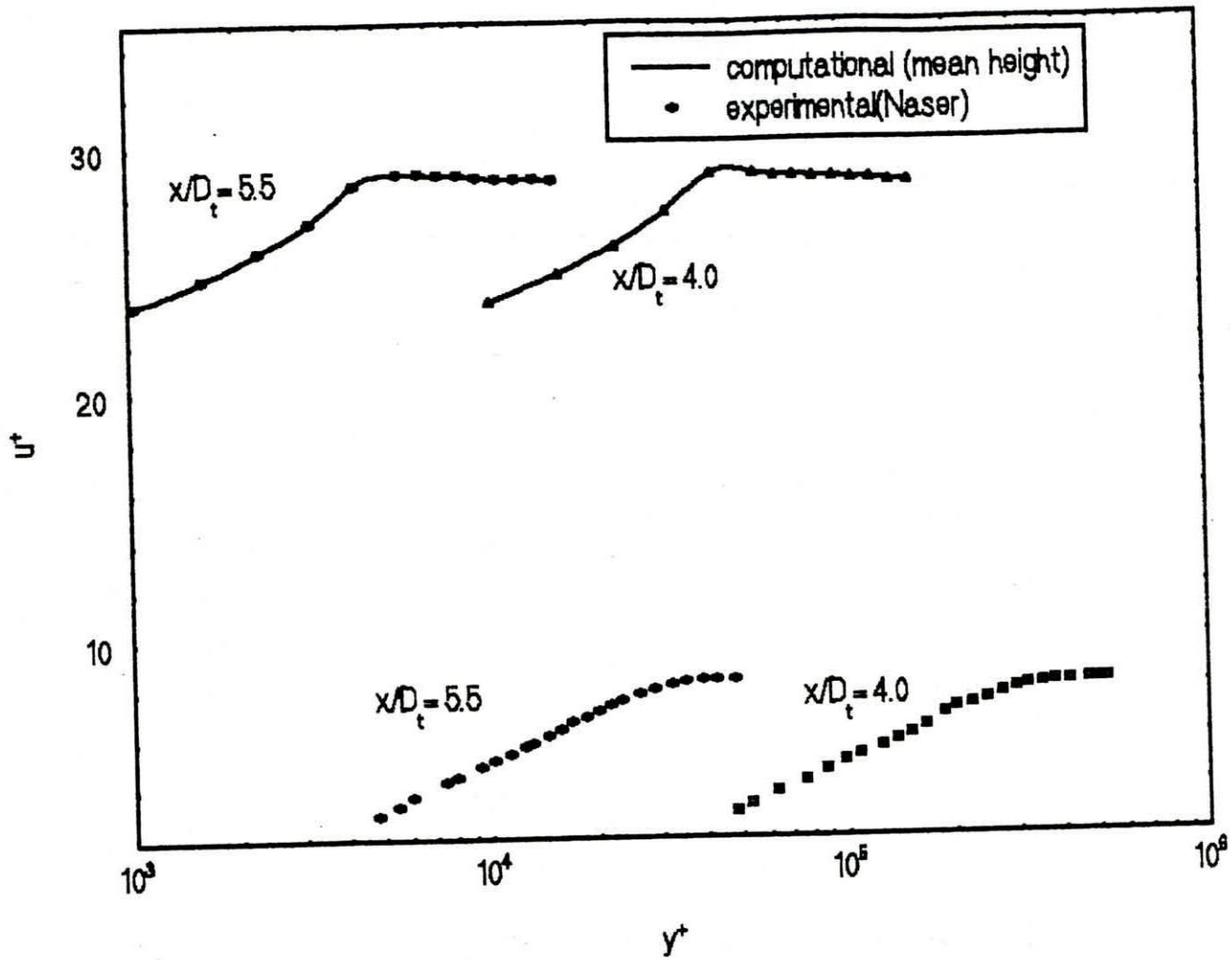

Fig. 4.8(b) Logarithmic velocity profile over the rough surface (Mean-height)

APPENDIX-A

Structure of the Mathematical foundation

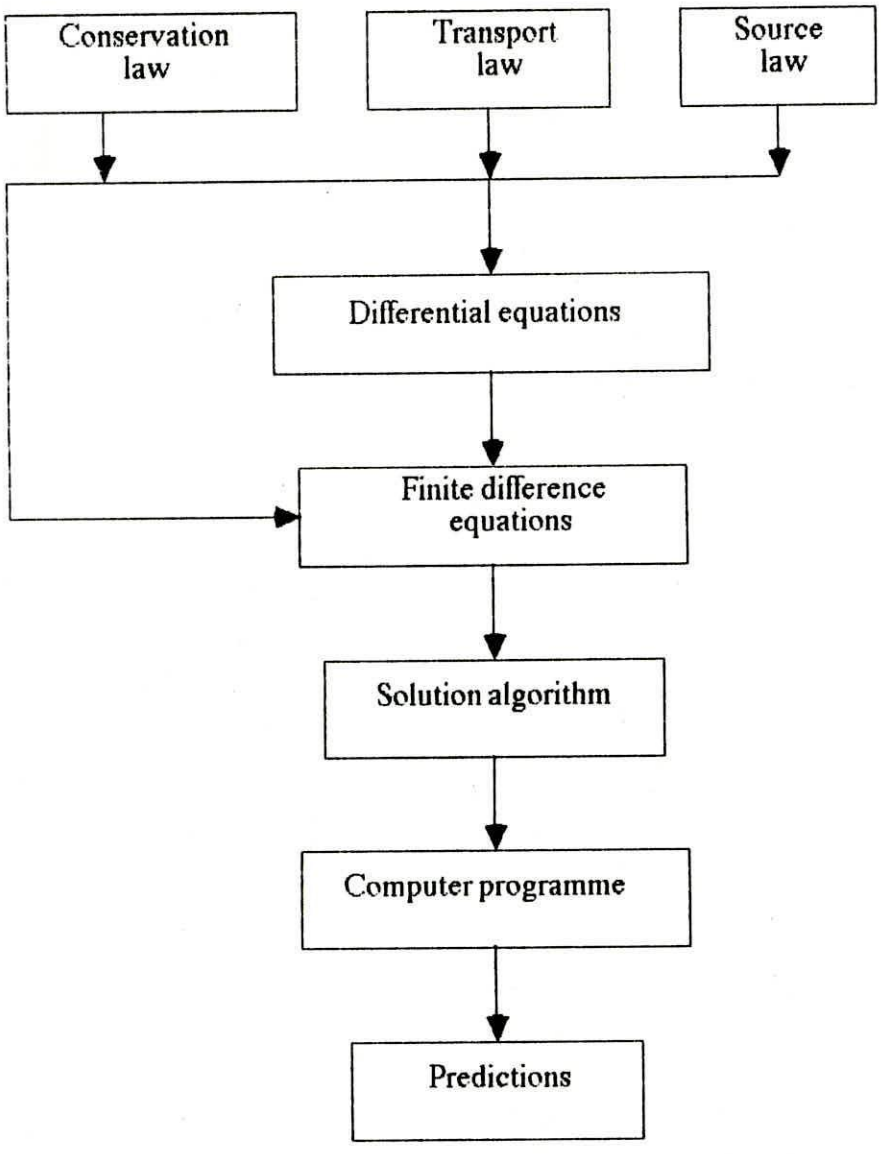

APPENDIX-B

The overall structure of TEACH - T